NANO · MICRO small
www.small-journal.com

Folate Receptor-Mediated Delivery of Cas9 RNP for Enhanced Immune Checkpoint Disruption in Cancer Cells

Yi Lin, Ulrich Wilk, Jana Pöhmerer, Elisa Hörterer, Miriam Höhn, Xianjin Luo, Hongcheng Mai, Ernst Wagner, and Ulrich Lächelt**

The clustered regularly interspaced short palindromic repeats (CRISPR)/CRISPR-associated protein 9 (Cas9) system offers great opportunities for the treatment of numerous diseases by precise modification of the genome. The functional unit of the system is represented by Cas9/sgRNA ribonucleoproteins (RNP), which mediate sequence-specific cleavage of DNA. For therapeutic applications, efficient and cell-specific transport into target cells is essential. Here, Cas9 RNP nanocarriers are described, which are based on lipid-modified oligoamino amides and folic acid (FolA)-PEG to realize receptor-mediated uptake and gene editing in cancer cells. In vitro studies confirm strongly enhanced potency of receptor-mediated delivery, and the nanocarriers enable efficient knockout of GFP and two immune checkpoint genes, PD-L1 and PVR, at low nanomolar concentrations. Compared with non-targeted nanoparticles, FolA-modified nanocarriers achieve substantially higher gene editing including dual PD-L1/PVR gene disruption after injection into CT26 tumors in vivo. In the syngeneic mouse model, dual disruption of PD-L1 and PVR leads to CD8+ T cell recruitment and distinct CT26 tumor growth inhibition, clearly superior to the individual knockouts alone. The reported Cas9 RNP nanocarriers represent a versatile platform for potent and receptor-specific gene editing. In addition, the study demonstrates a promising strategy for cancer immunotherapy by permanent and combined immune checkpoint disruption.

1. Introduction

The clustered regularly interspaced short palindromic repeats (CRISPR)/CRISPR-associated protein 9 (Cas9) technology, originally discovered as a type of bacterial adaptive immune system, is a groundbreaking genetic engineering tool that enables editing of genes by introducing double-strand breaks (DSB) at target genomic loci.[1] In clinical applications, well designed gene modifications can translate into permanent therapeutic effects and potentially constitute a cure for certain diseases. For the treatment of cancer, the current main application in clinical trials is ex vivo engineering of immune cells for adoptive cell therapies.[2] These approaches are based on immune checkpoint blockade (ICB) which counteracts the inhibition of immune reactions and reverts tumor-induced immune suppression.[3] Based on a similar strategy, monoclonal antibodies (mAbs) targeting immune checkpoint molecules are already well-established ICB agents in the clinic[4] and several therapeutics, such as anti-cytotoxic T lymphocyte-associated antigen 4 (CTLA-4),[5] anti-programmed cell death-1 (PD-1),[6] and anti-programmed cell death ligand-1 (PD-L1) inhibitors,[7] have been approved by the authorities. Due to the great success and dynamic nature of the field, it can be expected that new cancer immunotherapies will emerge, based on alternative targets or blockade mechanisms.

T cell immunoreceptor with immunoglobulin (Ig) and immunoreceptor tyrosine-based inhibitory motif domain (TIGIT)/poliovirus receptor (PVR) is a newly identified checkpoint axis that emerged as a promising immunological target.[8] Blockade of the TIGIT/PVR axis has been found to reverse T cell exhaustion and enhance antitumor efficacy in diverse types of cancer, including breast cancer,[9] hepatocellular carcinoma,[10] head and neck squamous cell carcinoma,[11] colorectal carcinoma,[12] and melanoma.[13] Moreover, PVR has been identified as an

Y. Lin, U. Wilk, J. Pöhmerer, E. Hörterer, M. Höhn, X. Luo, E. Wagner, U. Lächelt
Department of Pharmacy and Center for NanoScience (CeNS)
LMU Munich
81377, Munich, Germany
E-mail: ernst.wagner@cup.uni-muenchen.de; ulrich.laechelt@univie.ac.at

The ORCID identification number(s) for the author(s) of this article can be found under https://doi.org/10.1002/smll.202205318.

DOI: 10.1002/smll.202205318

H. Mai
Institute for Tissue Engineering and Regenerative Medicine (iTERM)
Helmholtz Zentrum München
85764, Neuherberg, Germany

H. Mai
Institute for Stroke and Dementia Research (ISD)
University Hospital
LMU Munich 81377, Munich, Germany

U. Lächelt
Department of Pharmaceutical Sciences
University of Vienna
Vienna 1090, Austria

oncogene with high expression levels in numerous cancers[14] which promotes invasion, migration, proliferation, and angiogenesis.[15] It was demonstrated in several mouse tumor models, that PVR knockdown can inhibit tumor growth and reduce metastatic burden.[15a,b,16]

Utilizing the CRISPR/Cas9 system for immunotherapy can have several advantages: it offers the opportunity to permanently disrupt inhibitory genes and to induce durable therapeutic immune responses;[17] on the other hand, specific knockout of immune checkpoint genes in cancer cells can help to reduce systemic immune-related adverse events (irAEs).[18] Taken together, direct CRISPR/Cas9 editing of cancer cells with dual disruption of the immune checkpoints PD-L1 and PVR could be a promising strategy for cancer immunotherapy.

The CRISPR/Cas9 system can be applied by using different forms of biomolecules: pDNA, mRNA/sgRNA, or Cas9/sgRNA ribonucleoproteins (RNP).[19] The utilization of pre-assembled RNP is generally considered a straightforward and efficient approach, but also requires suitable delivery systems for successful transport into target cells.[19,20] Receptor-mediated delivery is highly desirable, since it increases safety and the specificity for individual target cells depending on the receptor expression levels.[21] Here, we present the development of synthetic Cas9 RNP nanocarriers which enable receptor-mediated cellular delivery of the genome editing machinery. The carriers are based on sequence-defined oligo(ethylenamino) amides (OAAs)[22] constructed from natural and artificial amino acids. In the past, this class of ionizable oligomers has already demonstrated high utility for the delivery of a variety of biomacromolecules, including pDNA,[23] siRNA,[24] mRNA,[25] proteins,[26] and phosphorodiamidate morpholino oligomers (PMOs).[27] A previous study identified a T-shape lipo-OAA containing hydroxystearic acid (T-OHSteA) as a potent structure for Cas9 RNP delivery.[28] In the current work, we present the realization of folate receptor α (FRα)-mediated Cas9 RNP delivery, via click chemistry modification of the nanocarriers,[29] for potent gene knockout in FRα expressing cancer cells and dual PD-L1/PVR immune checkpoint disruption at tumor sites (**Scheme 1**).

2. Results and Discussion

2.1. Cas9 RNP Nanocarrier Design and Characterization

The hydroxystearyl oligo(ethylenamino) amide #1105 was previously identified as a potent structure for intracellular delivery of Cas9 RNP.[28] To enable the post-functionalization with receptor ligands by click chemistry, an analog with azido function at the *N*-terminus, oligomer #1445, was synthesized by solid-phase-supported synthesis (SPS, **Figure 1**a). Azides can readily react with dibenzocyclooctynes (DBCO) via strain-promoted azide-alkyne cycloaddition (SPAAC) in water and without the requirement of catalysts. The standard procedure for the synthesis of hydroxystearyl oligomers from oleic acid containing precursors contains a prolonged hydrolysis step which has to be followed by treatment with a reducing agent (tris(2-carboxyethyl)phosphine, TCEP), to break disulfide bonds of cystines.[30] Since the azide function in oligomer #1445 does not tolerate these conditions, the synthesis strategy had to be changed to circumvent side-reactions: hydroxystearic acid was a priori synthesized from oleic acid in solution and then coupled as the final building block during solid-phase synthesis (Figure S1, Supporting Information).

As shown in Figure 1b, three different formulations of Cas9 RNP nanocarriers were prepared. First, the unmodified nanocarrier core was produced by mixing the negatively charged Cas9/sgRNA RNP complexes with the positively charged oligomer #1445 at a nitrogen-to-phosphate (N/P) ratio of 24. The obtained formulation was subsequently functionalized with FolA-PEG$_{24}$-DBCO or PEG$_{24}$-DBCO via click chemistry to generate FolA-PEG- or PEG-modified nanocarriers. To explore the effect of ligand feed ratio on the physiochemical properties of the nanocarriers, different equivalents (eq) of DBCO ligands were conjugated and the size, polydispersity (PDI), and zeta potential of the nanocarriers were determined by dynamic light scattering (DLS) (Figure 1c–e). The unmodified nanocarrier core displayed well-defined sizes with a z-average of 166 nm (PDI of 0.11), which slightly increased to 180–260 nm after modification with 0.05 to 0.75 eq of DBCO ligands. Higher ratios above 1 eq led to aggregation, presumably due to increasing charge neutralization, as can be seen in the zeta potential measurements (Figure 1d). The zeta potential continuously decreased from + 15 to + 4 mV (PEG-modified) with an increasing modification ratio, which demonstrates the shielding effect of PEG.[31]

Ribogreen and agarose gel electrophoresis assays were performed, in order to confirm the encapsulation of Cas9/sgRNA RNP in the nanocarriers. The Ribogreen assay determined a sgRNA encapsulation efficiency of 89.5% for the unmodified nanocarrier (Figure S2, Supporting Information), which confirms the efficient loading of RNP into the nanocarriers. Moreover, modification with DBCO ligands (0.5 eq and 0.75 eq) did not affect the complex stability: 87.5% – 91.6% of encapsulation efficiency were determined for all formulations. Consistent results were obtained by electrophoretic mobility shift assays, where all formulations showed complete gel retardation of RNP while smear bands were observed with naked sgRNA and RNP (Figure S3, Supporting Information). Transmission electron microscopy (TEM) measurements were further carried out to evaluate the appearance of the Cas9 RNP nanocarriers with or without 0.75 eq of ligand modification. All three formulations showed homogeneous and spherical particle shapes (Figure S4, Supporting Information). As expected, the particle sizes (approximately 50 nm) acquired from TEM were smaller than from DLS measurements due to the contribution of the dispersant to the hydrodynamic diameter in aqueous solution.[32]

2.2. Knockout Evaluation and Optimization

The overall in vitro gene editing efficiencies of the Cas9 RNP nanocarriers with or without FolA-PEG- or PEG-modification were evaluated by eGFP knockout in two different cancer reporter cell lines: FRα-positive colon carcinoma CT26 eGFP/luc and cervix carcinoma HeLa eGFP/tub cells (**Figure 2**). Incubation of the reporter cells with unmodified nanocarriers containing 75 nM RNP for 4 h induced 72.2% (CT26 eGFP/luc)

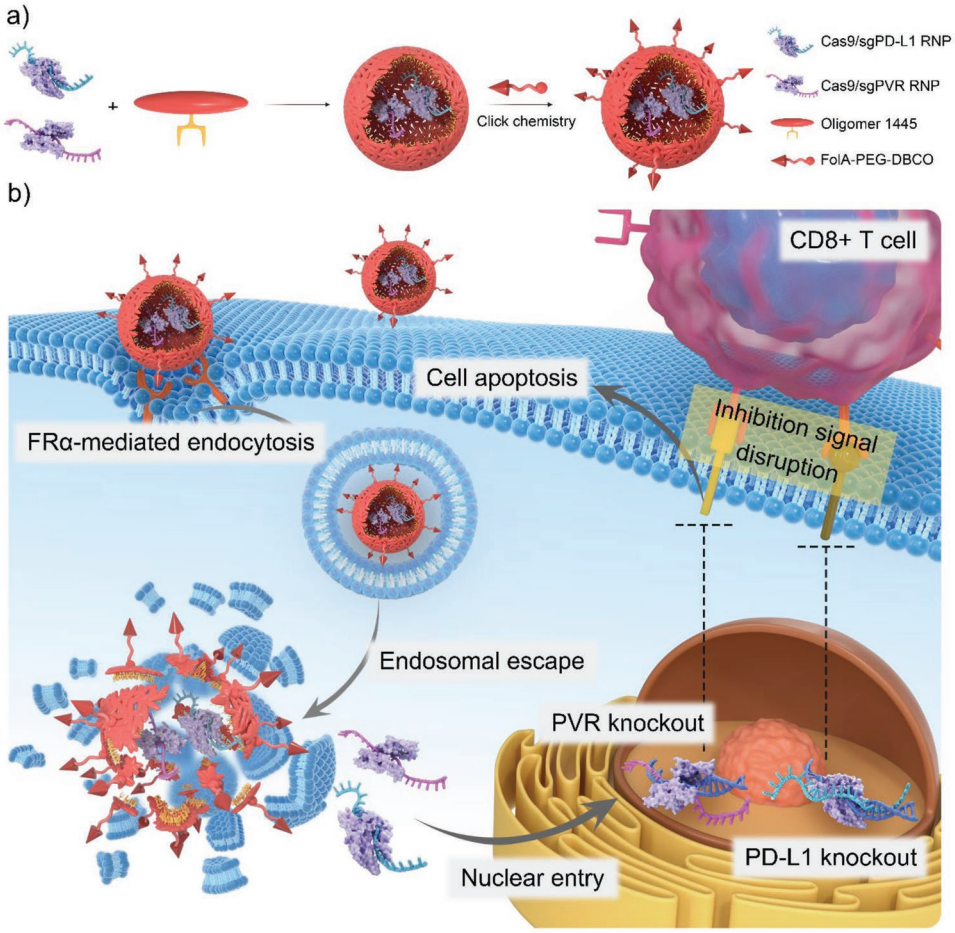

Scheme 1. FRα-specific Cas9 RNP nanocarriers for dual immune checkpoint disruption. a) Fabrication of folate receptor α (FRα)-specific Cas9 RNP nanocarriers targeting PD-L1 and PVR genes. An azide-containing T-shape oligomer is complexed with Cas9/sgPD-L1 and Cas9/sgPVR RNP and subsequently functionalized with folic acid (FolA)-PEG$_{24}$-DBCO (dibenzocyclooctyne) via click chemistry to form the FRα-specific dual RNP-loaded nanocarriers. b) Schematic illustration of receptor-mediated dual immune checkpoint disruption in FRα-overexpressing cancer cells. The FolA-modified nanocarriers are internalized via FRα and escape from endosomes. Finally, Cas9/sgPD-L1 and Cas9/sgPVR RNP enter the nucleus for simultaneous disruption of PD-L1 and PVR immune checkpoint genes which suppresses tumoral immune evasion (PD-L1), induces cell apoptosis, and inhibits cell proliferation (PVR).

and 67.2% (HeLa eGFP/tub) of eGFP knockout (Figure 2a). Modification with 0.75 eq PEG dramatically decreased the knockout efficiency in CT26 eGFP/luc cells (Figure 2a, left), indicating efficient PEG shielding, which suppresses unspecific cellular delivery.[33] In contrast, the knockout efficiency of FolA-PEG-modified nanocarriers was maintained at high levels despite similar surface modification with PEG. In contrast to the significant loss of activity due to PEG-conjugation, FolA-PEG-modified nanocarriers still mediated eGFP knockout of about 78.5% at the same modification ratio. This suggests, that the contained FolA restores the delivery efficiency of the well-shielded RNP nanocarriers. Similar tendencies were found in HeLa eGFP/tub cells, but 0.5 eq of PEG was already sufficient to achieve a clear PEG shielding effect (Figure 2a, right).

To investigate the effect of FRα-targeting on cellular delivery kinetics, cells were exposed to the Cas9 RNP nanocarriers for different durations between 15 min to 48 h and eGFP knockout was determined 5 days after the treatments (Figure S5, Supporting Information). In all cases, a general dependency of the knockout levels on the incubation time was observed, which is not surprising since longer exposure time increases the probability of cellular interactions and internalization. Notably, no significant differences were found between the 4 and 48 h incubation in case of the unmodified and FolA-PEG-modified carriers, which indicates that the uptake process is accomplished to a major extent within the first 4 h. FRα-targeted carriers clearly showed the best knockout efficiencies in CT26 eGFP/luc cells while PEG-modified was the worst and only achieved eGFP knockout levels of 28.5% after the longest incubation time of 48 h.

In HeLa eGFP/tub cells, FolA-PEG-modified nanocarriers with 2 h incubation already achieved similar eGFP knockout levels as the unmodified carriers after 4 and 48 h, which indicates an accelerated cellular delivery via FRα. To confirm that the observed advantages of FolA-modification are indeed receptor-specific, an FRα-negative cell line was generated from HeLa eGFP/tub via CRISPR/Cas9 knockout. The direct comparison of the HeLa eGFP/tub derivatives demonstrated

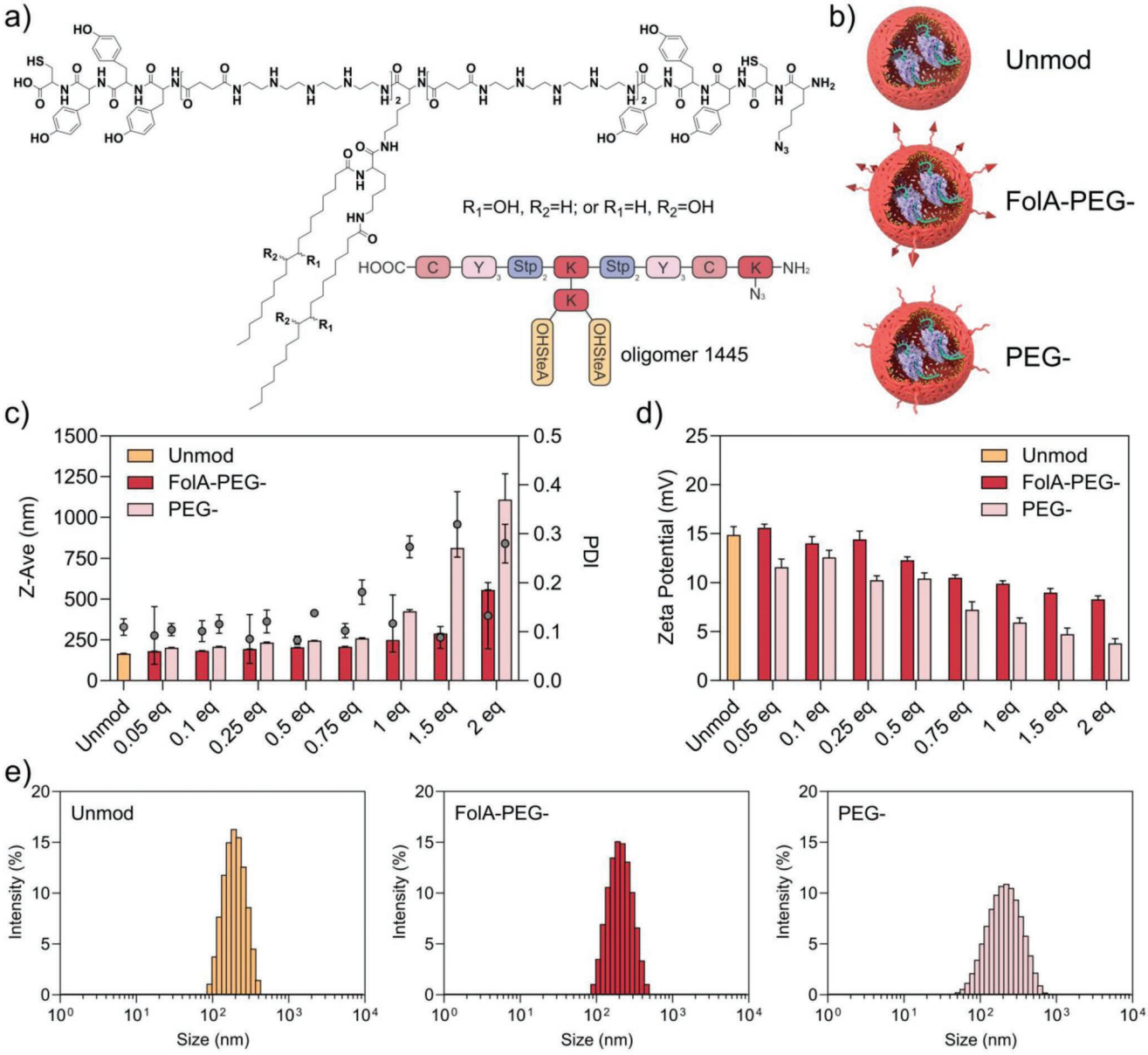

Figure 1. Characterization of Cas9 RNP nanocarriers. a) Chemical structure and sequence of T-shape oligomer #1445 with *N*-terminal azidolysine for functionalization with FolA-PEG_{24}-DBCO or PEG_{24}-DBCO via strain-promoted azide-alkyne cycloaddition (SPAAC). b) Schematic illustration of three different formulations of Cas9 RNP nanocarriers: unmodified, FolA-PEG- and PEG-modified nanocarriers. c) Hydrodynamic particle size (z-average), polydispersity index (PDI), and d) zeta potential of Cas9 RNP nanocarriers at different FolA-PEG- or PEG- to oligomer ratios (75 nM RNP). Three technical replicates were measured. e) Intensity size distribution of three different formulations of Cas9 RNP nanocarriers.

that FolA-modification mediates distinct enhancement of knockout levels in FRα-positive cells, whereas the advantage vanishes in FRα-negative cells. In the FRα-deficient cell line, the unmodified nanocarrier outperformed the FolA-PEG nanocarrier, which indicates that the advantages of FolA-PEG modification are highly specific and receptor-dependent.

To assess the effects of FRα-targeting on the potency more in detail, systematic dose-titration experiments with RNP concentrations from 1 to 100 nM were carried out (Figure 2b). All three formulations showed dose-dependent knockout activity in all three cell lines, but a clear dependency of the FolA-PEG nanocarrier on FRα-expression became obvious: the FolA-modified formulation has the highest potency in the cell lines which express the target receptor, but the potency drops in the FRα-knockout cells. In CT26 eGFP/luc cells, FolA-PEG-modified carriers achieved approximately 80% of eGFP knockout at a RNP dose as low as 10 nM, while the unmodified carriers achieved less than 20% at 10 nM and 32% at a RNP dose of 25 nM.

The cytotoxicity of Cas9 RNP nanocarriers was investigated in parallel during the described knockout experiments and the formulations were generally well-tolerated (Figures S6–S8,

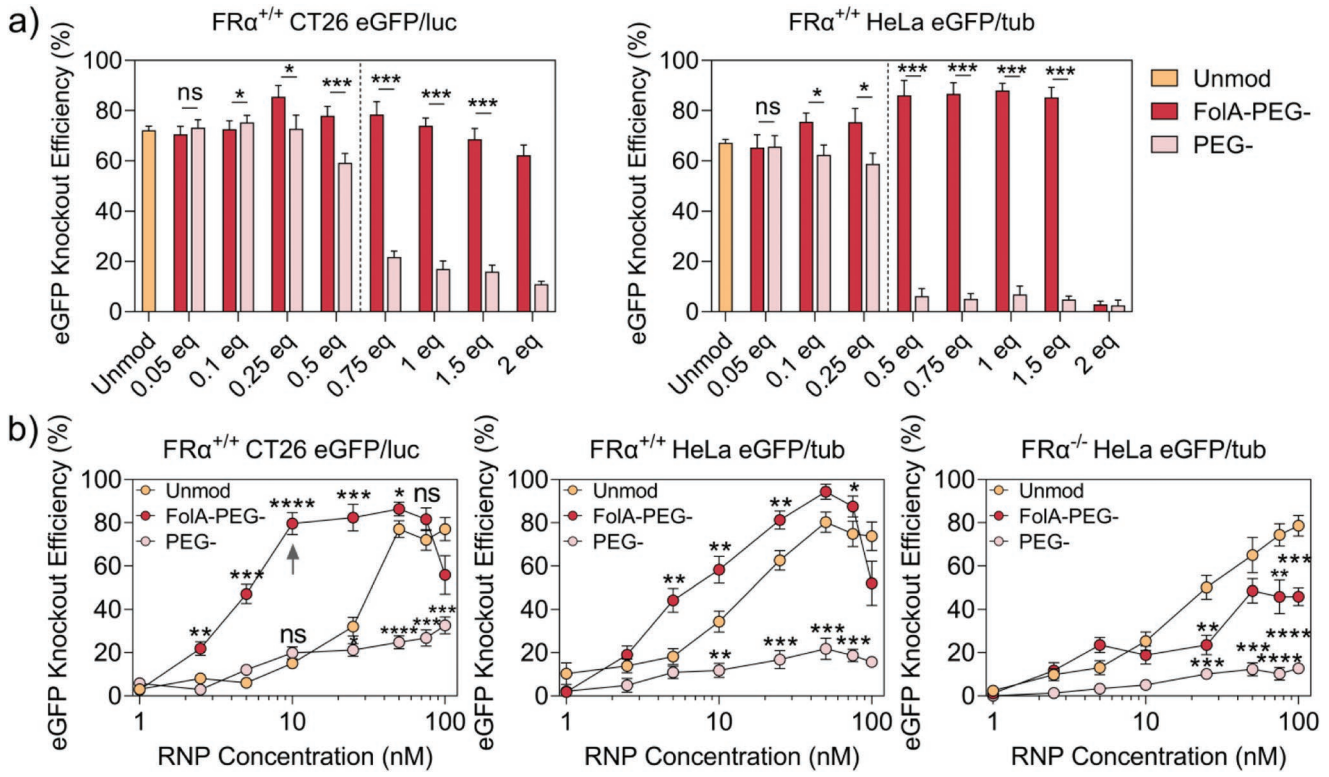

Figure 2. Knockout evaluation and optimization. a) eGFP knockout efficiency of Cas9 RNP nanocarriers at different FolA-PEG- or PEG- modification ratios in FRα-positive CT26 eGFP/luc and HeLa eGFP/tub cells. Cas9/sgGFP RNP was used at 75 nM. Cells were incubated with the formulations for 4 h followed by a medium change and evaluation after 5 days. b) Dose titration of Cas9 RNP nanocarriers containing 1 to 100 nM Cas9/sgGFP RNP in CT26 eGFP/luc cells (0.75 eq modification), HeLa eGFP/tub, or FRα-knockout HeLa eGFP/tub cells (0.5 eq modification). Cells were incubated with nanocarriers for 4 h and evaluation was performed 5 days after the treatment. Statistical significance was determined using the two-tailed student's t-tests in comparison to the unmodified nanocarrier at each concentration. ****$p \leq 0.0001$, ***$p \leq 0.001$, **$p \leq 0.01$, *$p \leq 0.05$; ns, not significant; Data are presented as mean ± SD (n = 3).

Supporting Information). Encouraged by the high potency and favorable characteristics of the Cas9 RNP nanocarriers, their stability during storage was evaluated, which generally is a critical parameter, but also an essential requirement for future applications. Cas9 RNP nanocarriers with or without 0.75 eq of ligand modification were prepared and directly stored at 4, –20, and –80 °C or first freeze-dried and then stored at –80 °C for up to two months. No significant particle aggregation was observed in any case, only a slight size increase was detected with the unmodified and FolA-modified nanocarriers stored at 4 °C (Figure S9, Supporting Information). Besides, knockout experiments were performed to evaluate the effects of storage on eGFP knockout in HeLa eGFP/tub cells (Figure S10, Supporting Information). The overall knockout efficiency of the nanocarriers did not significantly change over time and it can be concluded that the formulations can be stored without change of characteristics, preferably in a frozen or freeze-dried state.

2.3. Cellular Uptake and Endosomal Escape

Cellular delivery of biomolecules with nanocarriers is a complex multileveled process. To elucidate the impact of the nanocarriers on different stages, we investigated their cellular uptake and endosomal escape ability. The cellular uptake after different incubation times (45 min, 2 h, and 4 h) was quantified by flow cytometry using ATTO647N-labeled Cas9 protein and Cy3-labeled sgRNA in FRα-positive CT26, HeLa, and FRα-knockout HeLa cells (**Figure 3**a and Figures S11 and S12, Supporting Information). The FolA-PEG-modified nanocarrier mediated the highest levels of cellular uptake in FRα-positive cells at each time point, while PEG-modified showed the lowest. In contrast, the advantage of FolA-PEG modification vanished in FRα-negative HeLa cells and the unmodified nanocarrier exhibited the strongest cellular uptake. All three formulations demonstrated time-dependent uptake characteristics. The maximal uptake levels in CT26 cells were obtained after 4 h, where the median fluorescence intensity (MFI) of labeled Cas9 mediated by the FolA-PEG carrier was threefold and sevenfold higher, and the sgRNA MFI fivefold and 13-fold higher than in the case of the unmodified or PEG-modified, respectively.

The intracellular localization at this time point was visualized by confocal laser scanning microscopy (CLSM) (Figure 3b). Consistent with the flow cytometry results, most intense red (Cas9) and green (sgRNA) signals were observed in FolA-PEG nanocarrier-treated cells. Altogether, these data confirm that the FolA-PEG modification realizes FRα-specificity and strongly enhances the cellular internalization in FR-α expressing cancer cells.

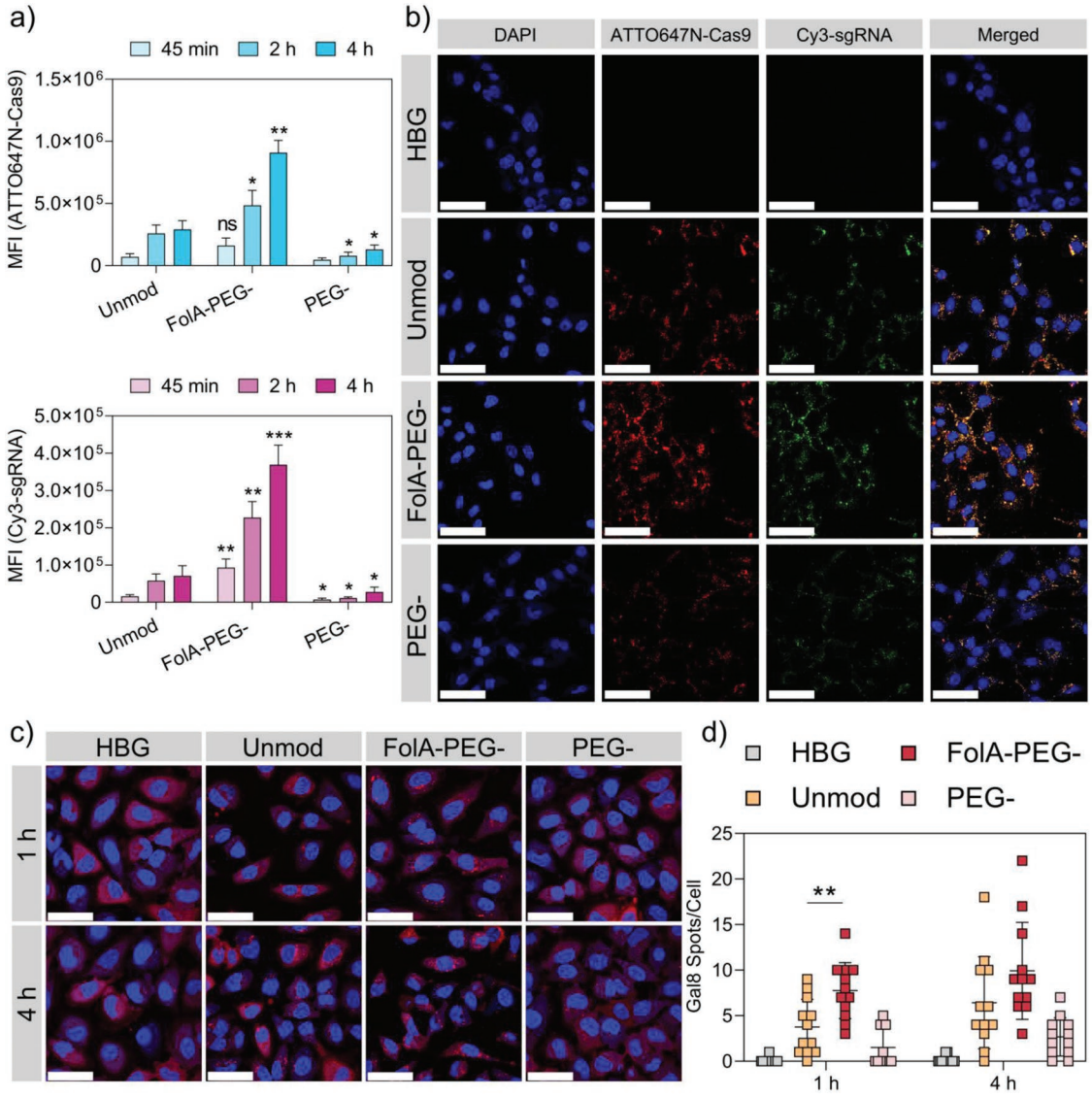

Figure 3. Cellular uptake and endosomal escape. a) Cellular uptake of Cas9 RNP nanocarriers (75 nM RNP, modification ratio 0.75 eq) containing 20% of ATTO647N-Cas9/Cy3-sgRNA into CT26 WT cells. Median fluorescence intensity (MFI) was determined by flow cytometry after 45 min, 2 h, and 4 h of incubation. Statistical significance was determined using the two-tailed student's t-tests in comparison to unmodified nanocarrier at each time point. $***p \leq 0.001$, $**p \leq 0.01$, $*p \leq 0.05$; ns, not significant. Data are presented as mean ± SD (n = 3). b) Confocal laser scanning microscopy (CLSM) images of CT26 WT cells after 4 h of treatment with Cas9 RNP nanocarriers (75 nM RNP, modification ratio 0.75 eq) containing 20% of ATTO647N-Cas9/Cy3-sgRNA. Nuclei were stained with DAPI (blue). The merged channel indicates co-localization (yellow) of ATTO647N-Cas9 (red) and Cy3-sgRNA (green). Scale bar: 70 µm. c) CLSM images of HeLa mRuby3/gal8 cells treated with Cas9 RNP nanocarriers (75 nM RNP, modification ratio 0.5 eq) for 1 and 4 h. Nuclei were stained with DAPI (blue). Red punctuate spots indicate damaged endosomes, due to binding of mRuby3/gal8 to ruptured endosomal membranes. Scale bar: 50 µm. d) Endosomal disruption levels after 1 and 4 h of treatment quantified by the number of mRuby3/gal8 spots per cell. HBG, HEPES-buffered glucose solution (20 mM HEPES, 5% glucose, pH 7.4). Data are presented as means ± SD (n = 12).

The endocytosis pathways, which are responsible for the internalization of the nanocarriers into CT26 and HeLa cells, were investigated by flow cytometry using Cy3-labeled sgRNA and different endocytosis inhibitors (4 °C incubation: energy-dependent endocytosis; chlorpromazine: clathrin-mediated endocytosis; nystatin: caveolae-mediated endocytosis; amiloride: macropinocytosis) (Figures S13 and S14, Supporting Information). Low temperature blocked the cellular uptake of all formulations by 80–90% in both cell lines, which suggests that energy-dependent endocytosis mechanisms play dominant roles in the uptake process of the RNP nanocarriers. In addition, chlorpromazine was the only inhibitor that was found to significantly suppress the uptake of unmodified and PEG-modified nanocarriers, indicating a clathrin-mediated endocytosis mechanism. Notably, both chlorpromazine (31.5% inhibition in CT26 and 29.5% in HeLa) and nystatin (23.1% inhibition in CT26 and 42.3% in HeLa) inhibited the cellular entry of the FolA-PEG nanocarrier. Based on these observations, a contribution of both clathrin- and caveolae-mediated endocytosis is assumed for the internalization of FolA-modified RNP

nanocarriers, which is consistent with the knowledge that the uptake of free folate proceeds via caveolae,[34] and in case of folate-conjugates converges with a pathway utilized by clathrin-coated pits.[35]

To characterize the endosomal escape capability of RNP nanocarriers, a HeLa cell line with stable expression of a mRuby3/galectin-8 (gal8) fusion protein was established using the PiggyBac transposon system together with a mRuby3/gal8 encoding plasmid.[36] The fluorescent galectin fusion proteins distribute in the cytosol when endosomal membranes are intact, and specifically bind to glycosylation moieties which are exposed when endosomes are ruptured.[37] Consequently, the recruitment of mRuby3/gal8 to endosomal membranes results in punctate red spots which are an indicator of damaged endosomes. HeLa mRuby3/gal8 cells were visualized by CLSM after 1 and 4 h of treatment with Cas9 RNP nanocarriers (Figure 3c) and the number of punctuate spots was counted per cell to quantify the endosomal escape capability (Figure 3d). The images reveal that the largest quantity of red spots appeared in cells treated with FolA-PEG-modified nanocarriers, indicating that the most efficient endosome disruption was caused by this carrier. Since each carrier is based on the same ionizable oligomer backbone, the higher endosomal escape performance of the FolA-PEG-carrier is suggested to be due to the faster kinetic of cellular uptake and the higher amount of internalized carrier material accumulating in endosomes. Interestingly, the average number of endosomal membrane damage events detected for the FolA-PEG carrier after 1 h was comparable to the unmodified core at the latest time point after 4 h (Figure 3d), which is very consistent with the faster uptake kinetic and the knockout experiments, where 1 h incubation with FolA-PEG-modified nanocarriers reached the same knockout level as 4 h incubation with the unmodified core (Figure S5, Supporting Information).

2.4. Validation of PD-L1 Disruption

After confirmation of FRα-specific Cas9 RNP delivery with reporter cells, the nanocarriers were utilized to induce disruption of endogenous immune checkpoint genes in wild-type cells. The first target was PD-L1, which was evaluated in CT26 cells after stimulation with 100 ng mL^{-1} interferon-γ (IFN-γ) (Figure S15, Supporting Information). Four sgRNAs targeting PD-L1 (Table S3, Supporting Information) were designed and tested with the nanocarriers at a RNP dose of 75 nM. sgPD-L1_4 that targets the exon 3 of murine PD-L1 gene (**Figure 4**a) was identified as the most efficient sgRNA sequence (Figure S16, Supporting Information). After 4 h treatment, the FolA-PEG-nanocarrier with sgPD-L1_4 induced 68.6% PD-L1 knockout, which was significantly higher than 38.2% and 13.2% achieved by the unmodified and PEG-conjugated carriers, respectively. Dose-titration experiments of the formulations revealed that the FolA-PEG-nanocarrier maintained high levels of PD-L1 knockout at RNP doses down to 25 nM, while the other two formulations immediately showed a dose-dependent reduction below 75 nM (Figure 4b,c). PD-L1 knockout was also visualized by CLSM after staining of CT26 cells with APC-labeled anti-PD-L1 antibody, which confirmed the advantage of FRα-mediated delivery (red, Figure 4d and Figure S17, Supporting Information).

Despite slight reduction of cell viability observed with the FolA-PEG-nanocarrier at high RNP doses, the formulations were generally well tolerated, as determined by cytotoxicity studies (MTT, Figure S18, Supporting Information). To validate the PD-L1 disruption at the genomic level, the insertions and deletions (Indels) causing PD-L1 gene knockout were investigated. Monoclonal cell lines were generated from CT26 cells 48 h after treatment by limiting dilution. The genomic DNA of the single cell-derived clones was extracted and the target region within PD-L1 exon 3 was amplified by PCR and determined by Sanger sequencing (Figure 4e). TIDE (Tracking of Indels by Decomposition) analysis was further carried out to determine the Indel frequency in the heterogeneous cell populations after treatments with the different nanocarriers (Figure 4f and Figure S19, Supporting Information). A total Indel frequency of 68.6% was estimated in cells treated with the FolA-PEG-modified nanocarriers, which was substantially higher than in the case of unmodified (40.7%) or PEG-conjugated (11.3%) nanocarriers. In conclusion, the data confirms that FRα-targeting enhances the Cas9 RNP delivery and enables efficient PD-L1 disruption in FRα-expressing CT26 cells.

2.5. Validation of PVR Disruption

The second endogenous target is PVR (CD155), an immunological factor that is overexpressed in various types of tumors including colorectal cancer.[38] PVR has been reported to not only inhibit the function of T cells via TIGIT/PVR axis but also promote the proliferation and migration of tumor cells.[16] It was recently found that PVR knockdown induces cell apoptosis and inhibits cell growth in colon cancer cells.[16b] To verify, if CRISPR/Cas9-mediated knockout can induce similar antitumoral effects, three sgRNAs targeting the PVR gene (Table S3, Supporting Information) were designed and tested with Cas9 RNP nanocarriers. The effect of PVR disruption on cell proliferation was first investigated by MTT assay and colony formation assay. The results of the MTT assay revealed that each of the sgRNA Cas9 RNP nanocarriers mediated a substantial decrease of cell viability in a dose-dependent manner. sgPVR_3 targeting the exon 5 of PVR gene (**Figure 5**a) outperformed the other two sgRNAs in terms of higher tumor cell killing at high RNP doses (Figure 5b and Figure S20, Supporting Information). The RNP formulation containing a control sgRNA without a target sequence in the genome (sgCtrl) was well tolerated, which rules out any unspecific carrier toxicity effects. In contrast, the FolA-PEG carriers containing sgPVR_3 significantly affected cell viability and over 93% reduction was achieved at doses of 75 and 100 nM, which was clearly higher than in the case of the unmodified (84%) and PEG-modified (66%) carriers. Similar findings were obtained in colony formation assays, where both the size and number of colonies originating from FolA-PEG-carrier treated cells were the lowest (Figure S21, Supporting Information). An Annexin V-FITC/PI assay was performed to evaluate whether apoptosis induction is responsible for the potent tumor cell killing via PVR knockouts. Annexin V binds to phosphatidylserine (PS) exposed on the cell

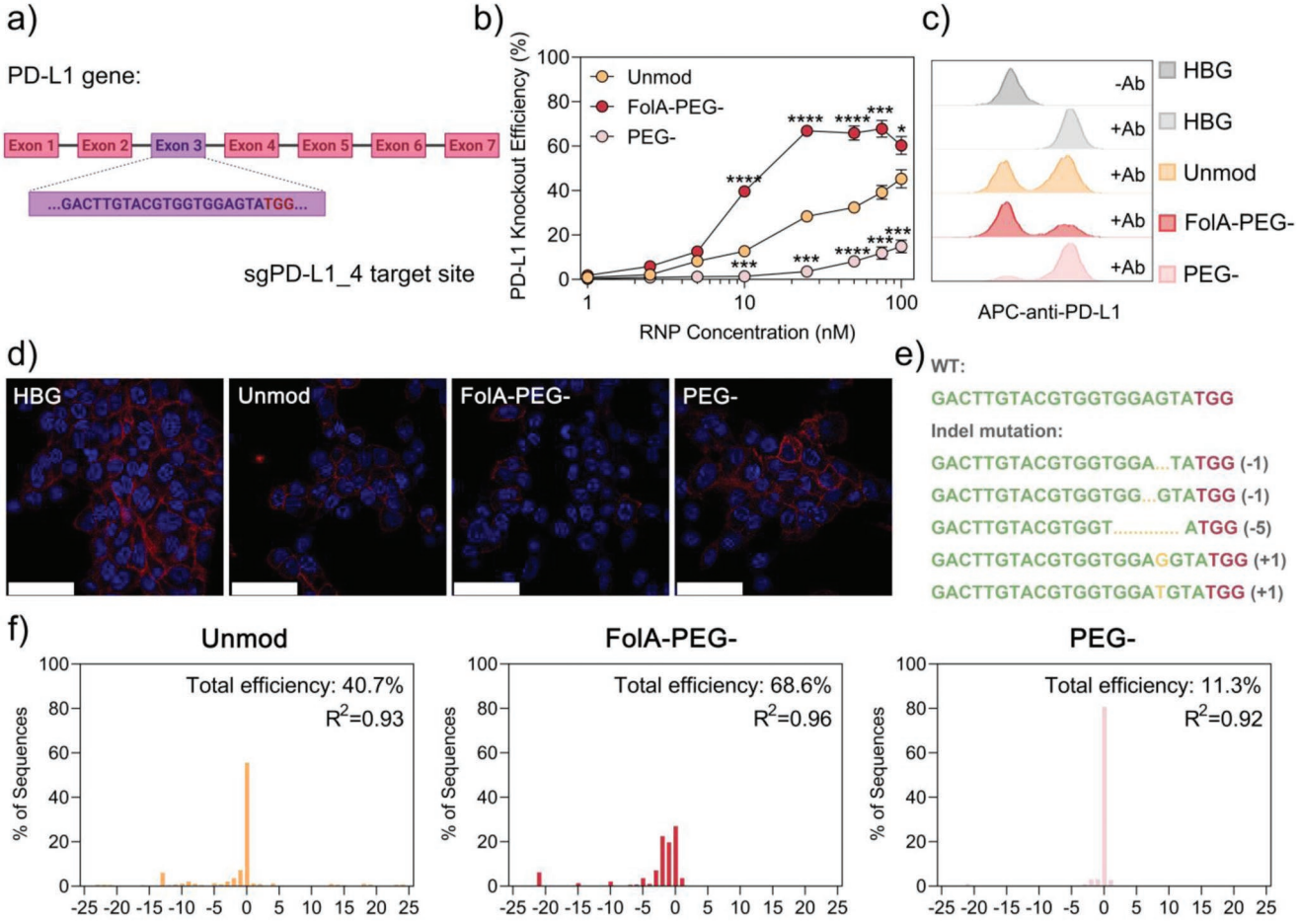

Figure 4. Validation of PD-L1 disruption. a) Exon map of the murine PD-L1 gene and the target region of sgPD-L1_4. b) PD-L1 knockout efficiency in a dose titration of Cas9 RNP nanocarriers containing 1 to 100 nM Cas9/sgPD-L1_4 RNP with or without modification at a ratio of 0.75 eq in CT26 WT cells. Nanocarriers were incubated with cells for 4 h followed by medium change and evaluation was performed 5 days after the treatment. Statistical significance was determined using the two-tailed student's t-tests comparing the knockout efficiency to the non-shielded group at each concentration. $^{****}p \leq 0.0001$, $^{***}p \leq 0.001$, $^{**}p \leq 0.01$, $^{*}p \leq 0.05$. Data are presented as mean ± SD (n = 3). c) Flow cytometry histograms and d) CLSM images showing the PD-L1 expression of CT26 WT cells after 4 h treatment with HBG buffer (20 mM HEPES, 5% glucose, pH 7.4), or Cas9 RNP nanocarriers (75 nM Cas9/sgPD-L1_4 RNP, 0.75 eq modification). Evaluation was performed 5 days after the treatment. For the detection of PD-L1, cells were treated with an allophycocyanin (APC)-conjugated antibody (Ab) against PD-L1. Nuclei were stained with DAPI (blue). Scale bar: 50 µm. Additional CLSM data including the full set of channels are provided in Figure S17, Supporting Information. e) Sequencing data of monoclonal PD-L1 knockout cells. The green sequence indicates the sgPD-L1_4 target sequence in exon 3 of the PD-L1 gene followed by the protospacer adjacent motive (PAM) in red. Detected insertions and deletions (Indels) are highlighted in orange. f) TIDE analysis of the sgPD-L1_4 target site of each group.

surface of early apoptotic cells; PI is able to pass through the damaged cell membranes of late apoptotic and necrotic cells and causes staining of DNA in the nucleus. Thus, Annexin V-positive and PI-negative cell populations indicate early apoptotic cells, whereas Annex V-positive and PI-positive suggest late apoptotic cells. As depicted in Figure 5c, most apoptotic events were detected in the cells treated with FolA-PEG-modified RNP carrier with a total of 57.4% apoptotic cells (19.8% early and 37.6% late apoptotic), while only 45.5% and 31.4% of apoptotic cells were detected in case of the unmodified and PEG-modified, respectively. To explore the time-resolved effects on proliferation and cell numbers, the cellular growth dynamics were investigated with a Cellwatcher real-time camera system (Figure 5d and Figure S22, Supporting Information). CT26 cells were constantly monitored up to 114 h by the Cellwatcher system (t = 0 to 144 h), which automatically identified the individual cells as indicated by the colored marks (Figure S22, Supporting Information). Different Cas9 RNP formulations were added 1 h after the start of recording (t = 1 h) and cell growth curves were generated based on the increasing cell confluency detected by the device (Figure 5d). The cells treated with buffer or sgCtrl RNP formulations all showed continuous cell proliferation until the end of the experiment, although at slightly different growth rates. In contrast, a flat curve was observed in case of the sgPVR containing formulations after a certain time point which indicates a stop of proliferation. Especially for the FolA-PEG-nanocarrier, an initial cellular growth was found in the first 12 h, which was followed by a rapid flattening to a constant level. At the endpoint of recording (t = 114 h), cells treated with FolA-PEG-nanocarriers containing sgPVR showed the lowest cell confluency.

The PVR expression levels after PVR knockout were determined by flow cytometry with PE-labeled anti-PVR

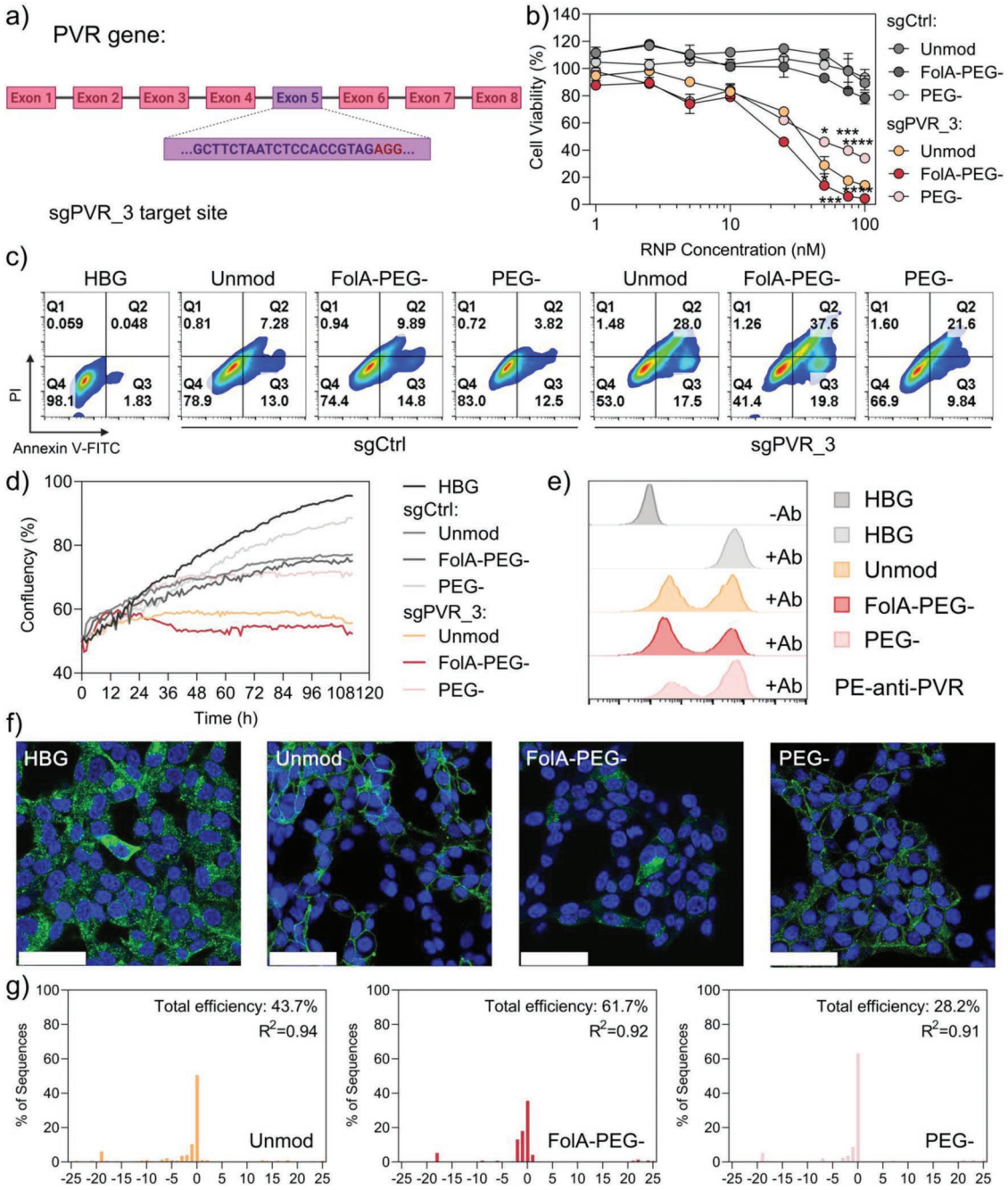

Figure 5. Validation of PVR disruption. a) Exon map of the murine PVR gene and the target region of sgPVR_3. b) Cell viability of CT26 WT cells treated with Cas9 RNP nanocarriers containing 1 to 100 nM Cas9/sgPVR_3 or sgCtrl (0.75 eq modification). Nanocarriers were incubated with the cells for 4 h followed by medium change and evaluation was performed 48 h after the treatment. Statistical significance was determined using the two-tailed student's t-tests in comparison to the unmodified nanocarrier at each concentration. $^{****}p \leq 0.0001$, $^{***}p \leq 0.001$, $^{**}p \leq 0.01$, $^{*}p \leq 0.05$. Data are presented as mean ± SD (n = 3). c) Apoptosis induction by Cas9/sgPVR_3 nanocarriers as determined by flow cytometry with Annexin V-FITC/PI staining. CT26 WT cells were treated with HBG buffer (20 mM HEPES, 5% glucose, pH 7.4), or Cas9 RNP nanocarriers (75 nM Cas9/sgPVR_3 or sgCtrl, 0.75 eq modification). Q1: necrotic cells; Q2: late apoptotic cells; Q3: early apoptotic cells; Q4: live cells. d) Cell growth dynamics of CT26 WT cells treated with HBG buffer, or Cas9 RNP nanocarriers (75 nM Cas9/sgPVR_3 or sgCtrl RNP, 0.75 eq modification) determined by a Cellwatcher system. Cas9 RNP nanocarriers were added 1 h after the start of recording. Additional Cellwatcher data are provided in Figure S22, Supporting Information. e) Histograms of flow cytometry and f) CLSM images showing the PVR expression of CT26 WT cells after 4 h treatment with HBG buffer, or Cas9 RNP nanocarriers (25 nM Cas9/sgPVR_3 RNP, 0.75 eq modification). Flow cytometry was carried out at day 4, CLSM at day 3 after transfection. PVR was stained with PE-labeled anti-PVR antibody (green), and nuclei with DAPI (blue). Scale bar: 50 µm. Additional flow cytometry and CLSM data are provided in Figures S23–S26, Supporting Information. g) TIDE analysis of the sgPVR_3 target site of each group.

antibody on day 3 and day 4 after Cas9 RNP nanocarrier treatments. On day 3 already two populations representing PVR-negative and PVR-positive cells were observed, but were not well separated (Figure S23, Supporting Information). A more reliable quantification was possible at day 4, where 62.6% PVR knockout was detected in the case of FolA-PEG-nanocarrier treated cells, while 50.3% and 32.5% were found in the case of unmodified and PEG-modified, respectively (Figure 5e and Figure S24, Supporting Information). Accordingly, the enhanced PVR gene disruption via FRα-mediated delivery was also confirmed by immuno-staining of PVR in CLSM imaging experiments (Figure 5f and Figure S25, Supporting Information). To exclude, that the reduced PVR expression was a consequence of the observed apoptosis, CT26 cells were treated with different apoptosis-inducing agents (doxorubicin, etoposide, cycloheximide) for 24 h and the occurrence of apoptotic events as well as PVR expression levels were determined. Encouragingly, the expression of PVR was not affected by the chemical induction of apoptosis (Figure S26, Supporting Information).

Finally, PVR knockouts were also confirmed at the genomic level. Since PVR disruption inhibits cell proliferation and induces apoptosis, the generation of PVR knockout clones is sophisticated. Thus, the genomic DNA of heterogenous cell populations 3 days after treatments was isolated, the genomic target site was amplified by PCR and analyzed via Sanger sequencing. TIDE analysis determined a total Indel frequency of 43.7% and 28.2% in the case of cells treated with unmodified and PEG-modified nanocarriers, respectively (Figure 5g and Figure S27, Supporting Information). Again, the FolA-PEG-nanocarrier mediated the highest frequency of 61.7%, which is very consistent with the PVR knockout levels determined by flow cytometry. Taken together, these data demonstrate that the FRα-specific Cas9 RNP nanocarriers enable the most efficient PVR disruption in CT26 cells, which leads to suppression of cell proliferation, induction of apoptosis, and cell killing.

2.6. Dual PD-L1/PVR Disruption In Vitro

After confirmation of single PD-L1 and PVR knockouts in CT26 cells, the dual PD-L1/PVR disruption by Cas9 RNP nanocarriers was evaluated. Cas9/sgPD-L1_4 and Cas9/sgPVR_3 RNP were encapsulated into the nanocarriers at an equimolar ratio (1:1) and a total RNP dose of 75 nM was used. Cells were treated for 4 h and the cell viability was evaluated by MTT assay 48 h later. Despite the lower amount of contained Cas9/sgPVR_3 RNP, the FRα-specific nanocarrier still reduced cell viability to 23%, which was significantly lower than the effects of the non-specific (**Figure 6**a). Flow cytometry determined 54.4% dual knockout of PD-L1 and PVR 72 h after the treatment with FolA-PEG-modified nanocarriers. In sum, 59.4% of cells showed any editing event (Figure 6b). In contrast, unmodified and PEG-modified Cas9 RNP carriers only mediated dual gene knockout at a frequency of 29.6% (37.6% total edits) and 19.3% (27.9% total edits), respectively. Interestingly, in all cases, the frequency of single knockouts of either PD-L1 or PVR was much lower than the dual knockout, which suggests that the developed RNP nanocarriers have a great potential for multiplexed genome editing. Figure 6c illustrates representative histograms obtained by flow cytometry of the treated cells, where dual knockout events are plotted at the bottom left while single PD-L1 and single PVR knockouts are found at the top left and bottom right, respectively.

The inhibited expression of PD-L1 (red) and PVR (green) induced by the different RNP carriers was also confirmed by CLSM experiments (Figure 6d). To further determine the dual knockout efficiency at the genomic level, TIDE analysis of the two target sequences was performed. The genomic DNA was isolated 3 days after treatments, and both PD-L1 and PVR target regions were amplified and analyzed by Sanger sequencing. As shown in Figure 6e and Figure S28, Supporting Information, 60.7% of PD-L1 and 58.7% of PVR Indel frequencies were determined in the case of cells treated with the FRα-specific nanocarriers, while 18.3% (PD-L1) and 21.9% (PVR) were observed for PEG-modified nanocarriers. The unmodified carrier core achieved medium levels of dual gene knockout with Indel frequencies of 31.7% (PD-L1) and 30.6% (PVR).

2.7. Dual PD-L1/PVR Disruption In Vivo

Once the potency of FRα-specific Cas9 RNP nanocarriers was confirmed in vitro, the capability to enable dual immune checkpoint disruption in vivo was assessed (**Figure 7**a). CT26 WT cells were inoculated subcutaneously into BALB/c mice. Three days later, Cas9 nanocarriers containing sgCtrl (25 µg sgCtrl per mouse), and sgPD-L1_4/sgPVR_3 (12.5 µg of each sgRNA per mouse) were injected intratumorally every other day with a total of 3 injections. Mice were euthanized 7 days after the last injection and single-cell suspensions were prepared from the tumors to determine PD-L1 and PVR expression levels by flow cytometry (Figure 7b and Figure S30, Supporting Information). The FolA-PEG-modified nanocarriers achieved around 25% of dual knockout and a total of 40% editing in the PD-L1 or PVR target loci in the tumors. The unmodified core showed lower efficiency with around 16% dual knockout and 25% total gene editing. Notably, only 4% of tumor cells were edited by the PEG-modified Cas9 RNP carriers. These results confirm that FRα-targeting also enhances the efficiency of Cas9 RNP delivery in the in vivo situation and is essential to achieve high potency. TIDE analysis of the genomic DNA from the tumor tissues confirmed that Indel frequencies of 33.2% in PD-L1 and 29.8% in PVR target loci were induced by FolA-PEG-modified Cas9 RNP carriers (Figure 6c and Figure S31, Supporting Information). Since the fundamental aim of immune checkpoint blockade therapy is the stimulation of the immune system against cancers, we investigated whether the dual PD-L1/PVR disruption does recruit cytotoxic T cells into the tumor microenvironment. The gating strategy of the flow cytometry evaluation to quantify CD8+ T cells is shown in Figure S32, Supporting Information.

Notably, the efficient dual PD-L1/PVR gene disruption by FolA-PEG-modified carriers significantly enhanced the infiltration of CD8+ T cells into the tumors in comparison to all other groups. These results demonstrate that the Cas9 RNP nanocarriers enable FRα-specific dual immune checkpoint disruption, which leads to CD8+ T cell recruitment in the tumors in vivo. Regarding the tolerability of the Cas9 RNP nanocarrier formulations, it is worth mentioning that no local irritation or

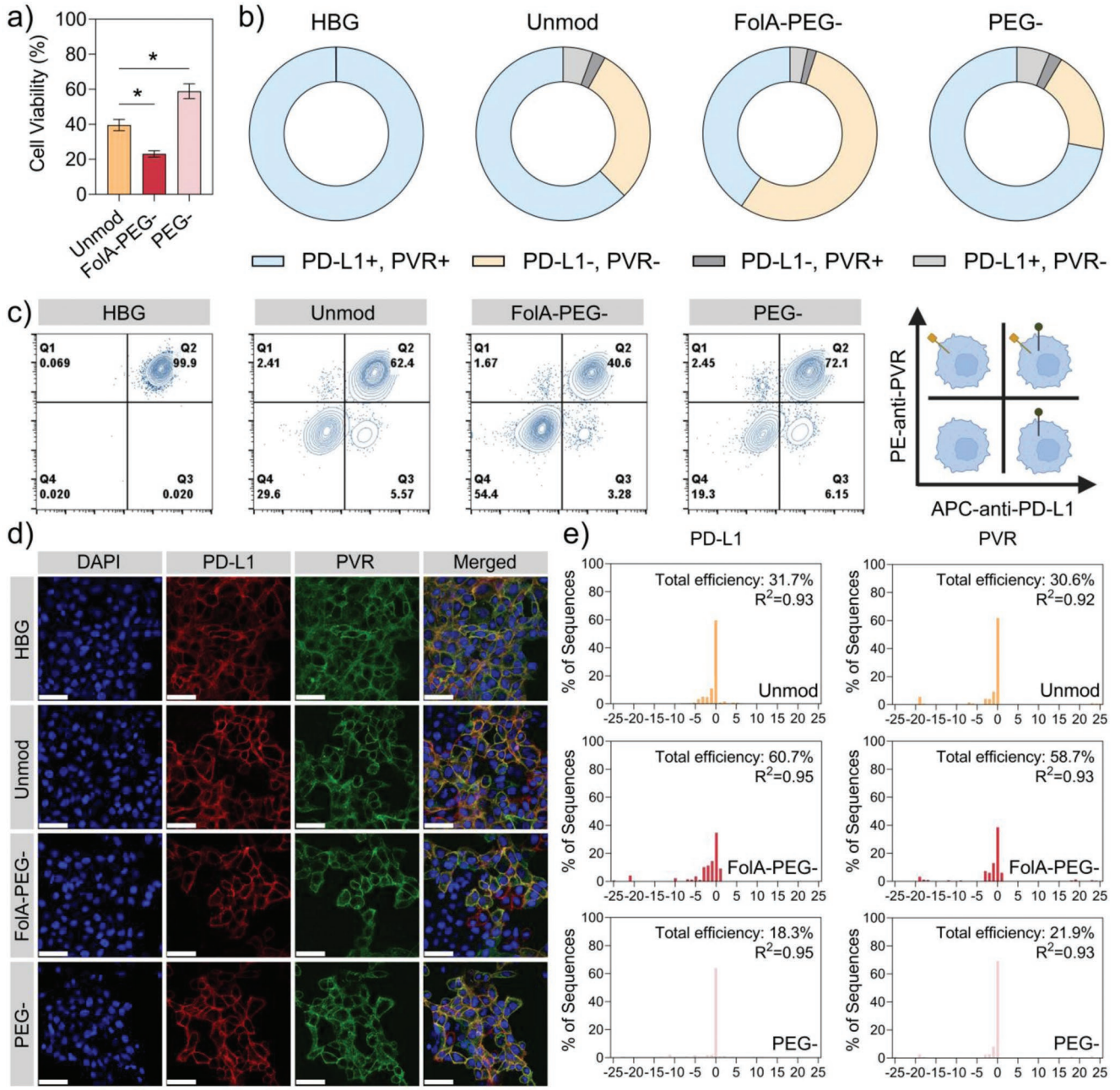

Figure 6. Dual PD-L1/PVR disruption in vitro. a) Cell viability and b) dual PD-L1/PVR knockout efficiency in CT26 WT cells treated with HBG buffer (20 mM HEPES, 5% glucose, pH 7.4) or nanocarriers containing 37.5 nM Cas9/sgPD-L1_4 and 37.5 nM Cas9/sgPVR_3 RNP (0.75 eq modification). Cas9 RNP nanocarriers were incubated with the cells for 4 h followed by medium change. MTT assay and flow cytometry were performed 48 and 72 h after the treatment, respectively. Statistical significance was determined using the two-tailed student's t-tests. *$p \leq 0.05$. Data are presented as mean ± SD (n = 3). c) Flow cytometry scatter plots and d) CLSM images showing the PD-L1 and PVR expression of CT26 WT cells after 4 h treatment with HBG buffer, or nanocarriers (37.5 nM Cas9/sgPD-L1_4 and 37.5 nM Cas9/sgPVR_3 RNP, 0.75 eq modification). Evaluation was performed 3 days after the treatments. PD-L1 was stained with APC-anti-PD-L1 (red), PVR with PE-anti-PVR (green) antibodies, and nuclei with DAPI (blue). Scale bar: 70 µm. e) TIDE analysis of sgPD-L1_4 (left) and sgPVR_3 (right) target loci of each group.

acute immune responses were observed upon subcutaneous injections at tumor-free sites (data not shown).

Finally, the resulting effects on tumor growth were evaluated in a separate therapeutic in vivo trial (**Figure 8**). CT26 WT cells were inoculated subcutaneously into BALB/c mice and RNP nanocarriers containing 25 µg sgRNA (sgCtrl, sgPD-L1_4/sgCtrl 1:1, sgPVR_3/sgCtrl 1:1, or sgPD-L1_4/sgPVR_3 1:1) and 0.75 eq of FolA-PEG modification were injected intratumorally at days 4, 7, 11, 18, 21, and 25 (Figure 8a). Tumor size and body weight of the mice were measured daily and animals were euthanized when tumors reached a critical size (≥ 12 mm in diameter) or when severe weight loss was observed.

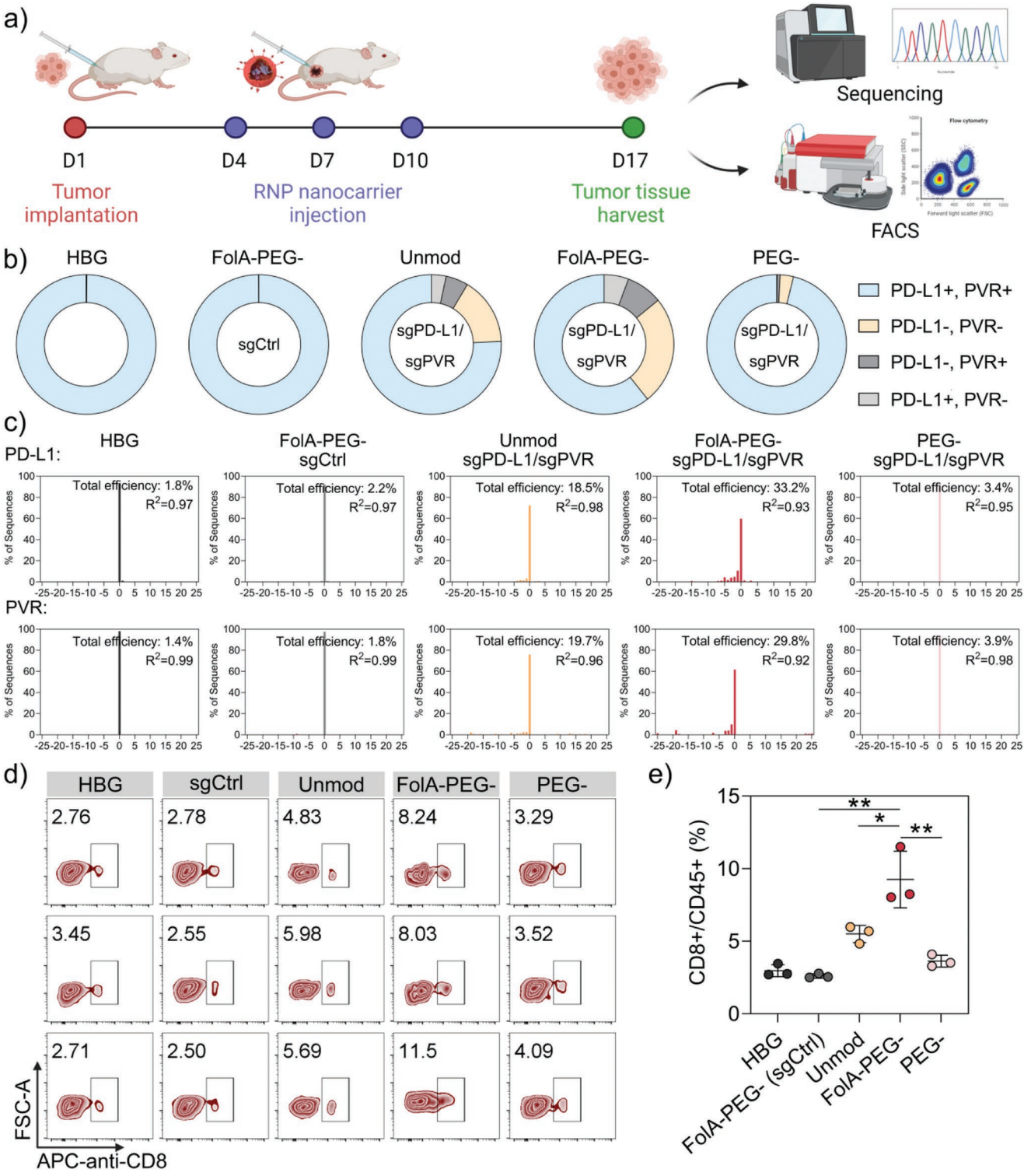

Figure 7. Dual PD-L1/PVR disruption in vivo. a) Schematic illustration of the experimental workflow. Different formulations of Cas9 RNP nanocarriers were administered intratumorally (i.t.) every other day with a total of 3 injections. Dual PD-L1/PVR knockout and CD8+ T cell recruitment at the tumor sites were evaluated 7 days after the last injection. b) PD-L1 and PVR knockout efficiencies as determined by flow cytometry of homogenized CT26 tumors treated with HBG buffer (20 mM HEPES, 5% glucose, pH 7.4) or Cas9 RNP nanocarriers containing Cas9/sgCtrl or Cas9/sgPD-L1_4 and Cas9/sgPVR_3 (1:1) (0.75 eq modification). c) TIDE analysis of sgPD-L1_4 and sgPVR_3 target loci of each group. Sanger sequencing data were evaluated by the TIDE web tool (http://tide.deskgen.com/). d) Flow cytometry scatter plots for quantification of CD8+ T cells. e) CD8+/CD45+ ratio for the determination of CD8+ T cell recruitment at the tumor sites. Statistical significance was determined using the two-tailed student's t-tests. $^{**}p \leq 0.01$, $^{*}p \leq 0.05$; Data are presented as mean ± SD (n = 3).

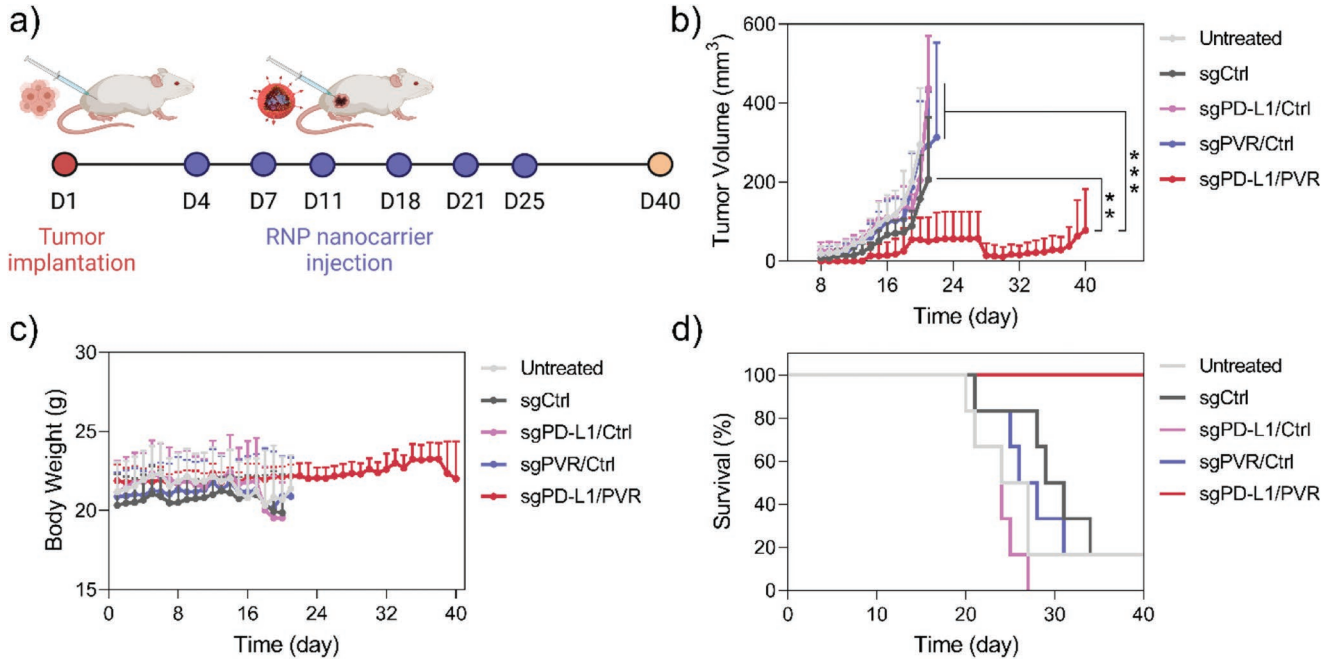

Figure 8. Antitumoral activity in vivo. a) Treatment schedule of Cas9 RNP nanocarriers in the syngeneic CT26 in Balb/c tumor model. Different formulations of Cas9 RNP nanocarriers were administered intratumorally (i.t.) at days 4, 7, 11, 18, 21, and 25. b) Tumor volume of subcutaneous CT26 tumors during the study. $^{**}p \leq 0.01$, $^{***}p \leq 0.001$; data are presented as mean ± SD (n = 5 for sgPD-L1+PVR group, n = 6 for other groups). c) Body weight of mice throughout the experiment. Data are presented as mean ± SD (n = 5 for sgPD-L1+PVR group, n = 6 for other groups). d) Kaplan–Meier survival curve of mice receiving different treatments.

Tumors of animals, which did not receive the Cas9 nanocarrier for dual immune checkpoint disruption (HBG, sgCtrl, sgPD-L1_4/sgCtrl, sgPVR_3/sgCtrl) showed continuous tumor growth beginning from day 8 (Figure 8b). Several mice from those groups had to be euthanized after day 20 due to exceeding tumor sizes or severe weight loss (Figure 8b,c). Neither sgCtrl nor single sgPD-L1 or sgPVR treatment showed significant inhibition of tumor growth (Figure 8b). In contrast, the tumor growth of dual sgPD-L1_4/sgPVR_3 treated mice was delayed (day 14) and strongly inhibited throughout the entire experiment. At day 20, the mean tumor size of the sgPD-L1_4/sgPVR_3 group was 2.9-, 3.7-, and fivefold smaller than those from the sgCtrl, sgPD-L1_4/sgCtrl, and sgPVR_3/sgCtrl groups, respectively. Besides, rather constant body weights were observed in the dual sgPD-L1_4/sgPVR_3 treated group. The Kaplan – Meier plot illustrates the improved survival rate of the dual sgPD-L1_4/sgPVR_3 treatment, where all mice survived at day 40 while at least 5 out of 6 animals were euthanized in all other groups (Figure 8d). Overall, the in vivo antitumor results demonstrate that dual PD-L1/PVR immune checkpoint disruption mediated by FRα-specific Cas9 RNP nanocarriers can significantly suppress tumor growth in vivo, providing a promising strategy for cancer immunotherapy.

3. Conclusion

In summary, an efficient and FRα-specific Cas9 RNP nanocarrier has been developed, which is based on a hydroxystearyl oligoamino amide (#1445) to permanently disrupt PD-L1 and PVR immune checkpoint genes in tumors. The FolA-PEG-modified Cas9 RNP nanocarriers mediated enhanced receptor-targeted cellular uptake and endosomal escape compared to unmodified and PEG-modified nanocarriers, resulting in more efficient and specific gene knockout in FRα-positive CT26 and HeLa cells in vitro as well as in CT26 tumors in vivo. In particular, potent PD-L1 and PVR gene knockout was achieved with the FolA-PEG-carrier in CT26 cells, and PVR disruption was found to strongly inhibit cell proliferation, and induce apoptosis and cell killing. Importantly, the FolA-PEG-modified Cas9 RNP carriers facilitated ≈25% of dual PD-L1/PVR knockout in CT26 tumors, induced CD8+ T cell recruitment into the tumor microenvironment, and achieved significant tumor growth inhibition. The therapeutic experiment demonstrated that dual disruption of PD-L1 and PVR genes are highly favorable to reduce tumor growth, which is consistent with literature reporting CT26 to be a model for non-hypermutated CRC tumors with lower neoantigen burden and lower response rate towards mono-therapy with anti-PD-L1 blocking antibodies, as compared to other CRC models.[39] In conclusion, the developed nanocarriers are suggested to constitute a highly efficient platform for receptor-specific delivery of Cas9 RNP with numerous potential applications. Furthermore, the presented dual immune checkpoint disruption strategy has the potential for the development of CRISPR/Cas9-based immunotherapies and cancer therapeutics in the future.

4. Experimental Section

Synthesis of Oligomer 1445: The synthesis of the artificial amino acid Fmoc-Stp(Boc)$_3$-OH (Stp) was described previously by Schaffert

et al.[40] First, the 1445 backbone of C(Trt)-[Y(tBu)]$_3$-[Stp(Boc)$_3$]$_2$-K(Dde)-[Stp(Boc)$_3$]$_2$-[Y(tBu)]$_3$-C(Trt)-Lys(N$_3$) (C → N) was synthesized manually using standard Fmoc solid-phase peptide synthesis conditions. Coupling step was performed using 4 eq Fmoc-amino acid, 4 eq HOBt, 4 eq PyBOP, and 8 eq DIPEA in DCM/DMF (1:1, 5 mL g^{-1} resin) for 75 min. Fmoc deprotection step was carried out by 3 times incubation with 20% piperidine in DMF (5 mL g^{-1} resin) for 15 min. After each coupling and deprotection step, the resin was washed 3 times with DMF and 3 times with DCM sequentially followed by a Kaiser test. After the last deprotection of Fmoc-Lys(N$_3$)-OH, the N-terminal NH$_2$-group was protected with 10 eq Boc$_2$O and 10 eq DIPEA in DCM/DMF (1:1, 5 mL g^{-1} resin). Dde deprotection step was accomplished by 15 times incubation with 2% hydrazine in DMF for 2 min. Afterwards, the resin was washed 5 times with DMF, 5 times with 10% DIPEA in DMF, and 3 times with DCM (5 mL g^{-1} resin each) sequentially. Subsequently, Fmoc-Lys(Fmoc)-OH was introduced followed by the coupling of hydroxystearic acid. The resin was washed 3 times with DMF and DCM sequentially and dried in vacuo. The oligomer was cleaved off the resin by incubation with pre-cooled cleavage cocktail TFA/EDT/H2O/TIS (94:2.5:2.5:1, 10 mL g^{-1} resin) for 60 min. The solution was immediately precipitated in pre-cooled MTBE/n-hexane (1:1, 45 mL). Afterwards, the oligomer was purified by gel filtration with an Äkta purifier system (GE Healthcare Bio-Sciences AB, Uppsala, Sweden) using a Sephadex G10 column and 10 mM HCl/ACN (7:3) as the mobile phase. The collected fractions were snap-frozen and lyophilized to obtain the final products.

Cas9 Protein Expression and Purification: Cas9 protein expression and purification were performed as described previously.[27] In brief, a plasmid pET28a/Cas9-Cys (pET28a/Cas9-Cys was a gift from Hyongbum Kim; Addgene plasmid no. 53261; http://n2t.net/addgene:53261; RRID: Addgene_53261)[41] was transformed into Rosetta 2(DE3)pLysS (Merck Millipore, Germany) as expression strain. An overnight culture was prepared from a monoclonal glycerol stock which was inoculated into LB medium containing kanamycin and chloramphenicol and incubated at 37 °C. Afterwards, the bacterial culture was diluted with LB medium (+kanamycin, +chloramphenicol) and incubated at 37 °C until an optical density at 600 nm (OD 600) of 0.5 – 0.7 was reached. Then, 1 mM isopropyl *β-D*-1-thiogalactopyranoside (IPTG) was added to the bacterial suspension to induce Cas9 protein expression, and the culture was incubated overnight at RT. On the next day, bacteria were harvested and resuspended in bacterial lysis buffer (20 mM trizma-base, 0.2 M NaCl, 20% sucrose, 10 mM $MgCl_2$, pH 7.5) followed by the addition of 30 µg mL^{-1} DNase, 10 µg mL^{-1} RNase, 1 mg mL^{-1} lysozyme, and 1 mM phenylmethylsulfonylfluoride (PMSF). The lysed suspension was frozen in liquid nitrogen, thawed on ice, and sonicated 3 times on ice for 20 s. The bacterial lysate was ultra-centrifuged (20 000 rpm) at 4 °C for 1 h followed by filtration using a syringe filter (0.45 µm).

The purification of Cas9 protein was performed by nickel chromatography (HisTrap HP column, GE Healthcare, Sweden). Afterwards, the collected fractions containing Cas9 were concentrated and further purified with an Äkta purifier using storage buffer (20 mM HEPES, 200 mM KCl, 10 mM $MgCl_2$, and 1 mM DTT) as the solvent. The fractions containing Cas9 were collected, and the concentration of Cas9 protein was measured with a Nanodrop photometer (Thermo Scientific, USA) using an extinction coefficient of $\varepsilon/1.000 = 120$ M^{-1} cm^{-1}. The Cas9 solution was aliquoted and stored at −80 °C.

Formulation of Cas9 RNP Nanocarriers: The Cas9 RNP complexes were formed by mixing the Cas9 protein with sgRNA at 1:1 molar ratio and incubation for 15 min at RT. The obtained RNP and the amount of oligomer 1445 corresponding to a N/P (nitrogen to phosphate) ratio of 24 were diluted separately with HBG (20 mM HEPES, 5% glucose, pH 7.4) to equal volumes. The RNP was added to the oligomer solution, mixed thoroughly by pipetting up and down, and finally incubated for 15 min at RT to give the final formulation. In case of the shielded and targeted formulations, the RNP nanocarriers were further conjugated with different DBCO agents (PEG$_{24}$-DBCO or FolA-PEG$_{24}$-DBCO). Varied equivalents (defined as molar ratios of DBCO agent to oligomer) of DBCO agents diluted in one-fourth volume of the RNP nanocarriers were added to the unmodified formulation, followed by 5 times pipetting up and down and 4 h incubation at RT.

Measurement of Particle Size and Zeta Potential: Dynamic and electrophoretic light scattering were applied for the determination of hydrodynamic particle size and zeta potential of Cas9 RNP nanocarriers. For the size measurements, 100 µL of RNP nanocarriers containing 1.25 µg Cas9 protein and 0.25 µg sgRNA (1:1 molar ratio) in HBG was measured 3 times with 13 sub-runs at a fixed scattering angle of 173°. Afterwards, 700 µL of HEPES buffer (20 mM, pH 7.4) was added to each sample, and zeta potential was analyzed 3 times with 12–15 sub-runs. All measurements were performed in folded capillary cells (DTS 1070) using a Zetasizer Nano ZS (Malvern Instruments, UK). The refractive index (RI) of the solvent was 1.330, the viscosity was 0.8872 mPa s, and the temperature was set to 25 °C.

Cell Culture: CT26 WT, CT26 eGFP/luc, HeLa eGFP/tub, FRα-knockout HeLa eGFP/tub, and HeLa mRuby3/gal8 cells were grown in DMEM medium supplemented with 10% FBS, 100 U mL^{-1} penicillin, and 100 µg mL^{-1} streptomycin. The cells were cultured in ventilated flasks in the cell incubator at 37 °C and 5% CO_2 in a humidified atmosphere. The cells were passaged at a confluency of approximately 80%.

FRα-knockout HeLa eGFP/tub cells were generated by using Cas9/sgFRα (Table S3, Supporting Information) ribonucleoproteins and a hydroxystearyl oligo(ethylenamino) amide #1105 as previously reported.[27] FRα-knockout single-cell derived lines were isolated by limiting dilution from the transfected pools. The detection of FRα was performed using allophycocyanin (APC)-conjugated α-FolR1 IgG$_1$ antibody by FACS. The genomic DNA of the identified FRα-negative cells was extracted and the sgFRα target regions of FRα gene were amplified with the FRα-F and FRα-R primers (see Table S5, Supporting Information). The knockout of FRα gene was further confirmed by sequencing the purified amplicons by Eurofins GATC Biotech (Germany) with the primer FRα-F. HeLa mRuby3/gal8 cells were generated as described below.

eGFP Reporter Gene Knockout by Flow Cytometry: One day prior to knockout experiments, CT26 eGFP/luc, HeLa eGFP/tub or FRα-knockout HeLa eGFP/tub cells were seeded into 96-well plates at a density of 5000 cells well^{-1}. On the next day, the medium in each well was replaced with 75 µL of fresh medium.

To optimize the FRα-specific gene knockout, 25 µL of RNP nanocarriers with or without different equivalents of FolA-PEG$_{24}$-DBCO or PEG$_{24}$-DBCO modification was added into each well resulting in a final concentration of 75 nM RNP complexes. For the dose titration experiment, RNP nanocarriers with or without 0.75 eq (CT26 eGFP/luc cells) or 0.5 eq (HeLa eGFP/tub cells) ligand modification were formulated and then diluted to prepare a series of different concentrations of RNP. 25 µL of dilutions were added to each well resulting in final concentrations of RNP ranging from 1 to 100 nM. To test the knockout efficiency after long-term storage, 25 µL of the samples were taken, eventually after reconstitution (freeze-dried sample), and then added into each well resulting in a final concentration of 75 nM RNP. After 4 h, the medium in each well was replaced with 100 µL of fresh medium and the cells were incubated for 44 h.

For optimizing the transfection time, RNP nanocarriers with or without 0.75 eq (CT26 eGFP/luc cells) or 0.5 eq (HeLa eGFP/tub cells) ligand modification were applied. The cells were incubated for different times (15 min, 30 min, 45 min, 1 h, 2 h, 4 h, or 48 h). After replacement with fresh medium, the cells were further incubated to reach the total incubation time of 48 h.

Afterwards, the cells were trypsinized and transferred to 24-well plates. After another 3 days of incubation, the cells were harvested and resuspended in 600 µL of FACS buffer. The samples were analyzed by flow cytometry on a CytoFLEX S flow cytometer (Beckman Coulter, CA, USA). Before the measurement, 1 ng µL^{-1} DAPI was added to differentiate between live and dead cells. The DAPI signal was detected with 405 nm excitation and 450 nm emission. The eGFP fluorescence was assayed with 488 nm excitation and 530 nm emission. Ten thousand isolated live cells were counted and evaluated. The data were analyzed using FlowJo 7.6.5 by FlowJo, LLC (Becton, Dickinson and Company, USA). All studies were performed in triplicate.

Cellular Uptake by Flow Cytometry: One day prior to the cellular uptake experiments, CT26 WT, HeLa WT, or FRα-knockout HeLa cells were

seeded into 24-well plates at a density of 25 000 cells well^{-1}. On the next day, the medium in each well was replaced with 375 µL of fresh medium. RNP nanocarriers with or without 0.75 eq (CT26 WT cells) or 0.5 eq (HeLa WT cells) ligand modification were prepared as described above using 20% of ATTO647N-Cas9 and 20% of Cy3-sgRNA. 125 µL of the nanocarriers was added to each well resulting in a final concentration of 75 nM RNP complexes. The cells were incubated for 45 min, 2 h, or 4 h. Afterwards, the cells were harvested, prepared, and analyzed by flow cytometry as described above. The DAPI signal was detected with 405 nm excitation and 450 nm emission. The ATTO647N fluorescence was assayed with 640 nm excitation and 670 nm emission. And the Cy3 fluorescence was detected with 550 nm excitation and 570 nm emission. All experiments were performed in triplicate.

Cellular Uptake by Confocal Laser Scanning Microscopy (CLSM): CT26 WT cells were seeded in 8-well Ibidi µ-slides (Ibidi GmbH, Germany) at a density of 15 000 cells well^{-1} 24 h prior to the treatment. On the next day, the medium was replaced with 225 µL of fresh medium. 75 µL of RNP nanocarriers containing 20% of ATTO647N-Cas9 and 20% of Cy3-sgRNA was added to each well resulting in a final concentration of 75 nM RNP. After 4 h, the medium was discarded and the cells were washed twice with 300 µL of PBS. Subsequently, 300 µL of PBS containing heparin (500 IU mL^{-1}) was added to disassociate extracellular nanocarriers from the cell membrane. The cells were incubated on ice for 20 min. Afterwards, the cells were washed with PBS followed by 40 min of fixation with 4% PFA at RT. The cells were then washed with PBS, and the cell nuclei were stained with DAPI (2 µg mL^{-1}). After 20 min incubation, the DAPI solution was removed. 300 µL of PBS was added per well for CLSM imaging. Images were recorded on a Leica-TCS-SP8 confocal laser scanning microscope equipped with a HC PL APO 63 × 1.4 objective (Germany). DAPI emission was recorded at 450 nm, ATTO647N-Cas9 at 670 nm, and Cy3-sgRNA at 570 nm. All images were analyzed using the LAS X software from Leica.

Gal8 Endosomal Escape Assay: HeLa cells with stable expression of a mRuby3-galectin 8 fusion protein were generated by using a Super piggyBac Transposase expression vector (SBI, CA, USA) and a PB-CAG-mRuby3-Gal8-P2A-Zeo plasmid.[33] The PB-CAG-mRuby3-Gal8-P2A-Zeo plasmid was a gift from Jordan Green (Addgene plasmid # 150815; http://n2t.net/addgene:150815; RRID:Addgene_150815). HeLa mRuby3/gal8 cells were seeded in 8-well Ibidi µ-slides (Ibidi GmbH, Germany) at a density of 15 000 cells well^{-1} 24 h prior to treatments. On the next day, the medium was replaced with 225 µL of fresh medium. 75 µL of RNP nanocarriers was added to each well resulting in a final concentration of 75 nM RNP. After 4 h, the cells were washed, fixed, stained, and imaged as described above. DAPI emission was recorded at 450 nm, mRuby3 emission was recorded at 590 nm. Gal8 spots per cell were analyzed using the ImageJ software.

Determination of Dual PD-L1/PVR Gene Knockout by Flow Cytometry: One day prior to the treatments, CT26 WT cells were seeded into 24-well plates at a density of 50 000 cells well^{-1}. On the next day, the medium in each well was replaced with 375 µL of fresh medium. Dual sgPD-L1/sgPVR loaded RNP nanocarriers with or without ligand modification (0.75 eq) were prepared as described above using sgPD-L1_4 and sgPVR_3 at a molar ratio of 1:1. 125 µL of RNP nanocarriers was added to each well resulting in a final concentration of 75 nM RNP in total. After 4 h, the medium in each well was replaced with 500 µL of fresh medium and the cells were incubated for 44 h. Afterwards, 100 ng mL^{-1} IFN-γ was added to each well to stimulate PD-L1 expression. After further incubation for 24 h, the cells were harvested, stained with APC anti-mouse PD-L1 antibody and PE anti-mouse PVR antibody, and analyzed by flow cytometry. All experiments were performed in triplicate.

Cell Viability Assay (MTT) After Dual PD-L1/PVR Gene Knockout: One day prior to the treatments, CT26 WT cells were seeded into 96-well plates at a density of 5000 cells well^{-1}. On the next day, the medium in each well was replaced with 75 µL of fresh medium. Dual sgPD-L1/sgPVR loaded RNP nanocarriers were applied and cells were incubated for 4 h. Afterwards, the medium was removed and 100 µL of fresh medium was added in each well. After 48 h total incubation, 10 µL of MTT (5 mg mL^{-1}) was added to each well. The cells were incubated for 2 h in the incubator. Afterwards, the medium was discarded, and the plates were frozen at –80 °C overnight. 100 µL of DMSO was then added to each well to dissolve the formed formazan product. The plates were incubated for 30 min at 37 °C under shaking. The absorbance of each well was measured at 590 nm with background correction at 630 nm using a microplate reader (Tecan Spark 10 M, Tecan, Männedorf, Switzerland). The relative cell viability (in percentage) was calculated relative to control wells treated with HBG buffer as ([A] test/[A] control) × 100%. All experiments were conducted in triplicate.

Determination of Dual PD-L1/PVR Gene Knockout by CLSM: One day prior to the treatments, CT26 WT cells were seeded in 8-well Ibidi µ-slides (Ibidi GmbH, Germany) at a density of 50 000 cells well^{-1}. On the next day, the medium was replaced with 225 µL of fresh medium. 75 µL of dual sgPD-L1/sgPVR loaded RNP nanocarriers was added to each well resulting in a final concentration of 75 nM RNP complexes. After 4 h, the medium in each well was replaced with 300 µL of fresh medium. The cells were further incubated for 44 h. Afterwards, 100 ng mL^{-1} IFN-γ was added to stimulate PD-L1 expression. After 24 h stimulation, the cells were stained using 2 µL of APC anti-mouse PD-L1 antibody and 2 µL of PE anti-mouse PVR antibody, washed, fixed, and imaged by CLSM as described above.

Sanger Sequencing and TIDE Analysis of Dual PD-L1/PVR Gene Edits: Genomic DNA of CT26 WT cells was extracted 3 days after treatments with dual sgPD-L1/sgPVR loaded RNP nanocarriers using a QIAamp DNA Mini Kit. The target regions of PD-L1 and PVR genes were amplified, gel purified, sequenced, and the TIDE web tool (http://tide.deskgen.com/) was used for evaluation of the Sanger sequencing data.

Dual PD-L1/PVR Gene Knockout In Vivo: All animal studies were performed according to guidelines of the German Animal Welfare Act and were approved by the animal experiments ethical committee of the "Regierung von Oberbayern", District Government of Upper Bavaria, Germany.

Eight-week-old, female, BALB/c mice, (Janvier, Le Genest-Saint-Isle, France), were housed in isolated ventilated cages under pathogen-free conditions with a 12 h light/dark interval and were acclimated for seven days prior to the treatments. Water and food were provided ad libitum. For the determination of the efficiency of dual immune checkpoint gene disruption in vivo, 5×10^5 CT26 WT cells were injected subcutaneously into the left flank. For the tumor growth inhibition study, 1×10^5 CT26 WT cells were injected subcutaneously into the left flank. The tumor volume was measured using a caliper and calculated as [0.5 × (longest diameter) × (shortest diameter)^2] and the body weight was recorded daily.

For dual gene knockout study, dual sgPD-L1/sgPVR loaded RNP nanocarriers containing 125 µg Cas9 protein, 12.5 µg sgPD-L1_4, and 12.5 µg sgPVR_3 with or without ligand modification (0.75 eq) were prepared in a total volume of 50 µL HBG. Control RNP nanocarriers containing 25 µg sgCtrl with FolA-PEG$_{24}$-DBCO modification were prepared in the same way. The mice were randomly divided into 5 groups (n = 6) 7 days after the tumor implantation. The RNP nanocarriers were intratumorally injected every other day with a total of 3 injections. The mice were euthanized by cervical dislocation 7 days after the last injection.

For tumor growth inhibition studies, sgCtrl (25 µg), sgPD-L1_4/sgCtrl (12.5 µg/12.5 µg), sgPVR_3/sgCtrl (12.5 µg/12.5 µg), or sgPD-L1_4/sgPVR_3 (12.5 µg/12.5 µg) loaded FolA-PEG$_{24}$-1445 RNP nanocarriers (125 µg Cas9 protein) were prepared in a total volume of 50 µL HBG. The mice were randomly divided into 5 groups (n = 5 for sgPD-L1/sgPVR group, n = 6 for other groups) 3 days after the tumor implantation. The RNP nanocarriers were intratumorally injected on days 4, 7, 11, 18, 21, and 25. The mice were euthanized by cervical dislocation when tumor reached the criteria of critical size (≥12 mm in diameter) or continuous weight loss occurred.

Flow Cytometry Analysis of Tumor Tissues: Tumor tissues were harvested, treated with FastPrep homogenizer, passed through 100 µm and subsequently 40 µm meshs, and washed with PBS to obtain single-cell suspensions.

To evaluate dual PD-L1/PVR gene knockout in vivo, 5 µL of APC anti-mouse PD-L1 antibody and 5 µL of PE anti-mouse PVR antibody were added to each sample (n = 3). The samples were incubated for 60 min on ice in the dark. Afterwards, the samples were washed, resuspended, and analyzed by flow cytometry as described above.

To evaluate CD8+ T cells recruitment, 5 µL of PE anti-mouse CD45 antibody and 5 µL of APC anti-mouse CD8 antibody (BioLegend, San Diego, CA, USA) were added to each sample (n = 3). The samples were incubated for 60 min on ice in the dark. Afterwards, the samples were washed, resuspended, and analyzed by flow cytometry as described above.

Sanger Sequencing and TIDE Analysis of Tumor Tissues: Genomic DNA of tumor tissues was extracted using a QIAamp DNA Mini Kit. The target regions of PD-L1 and PVR genes were amplified, gel purified, sequenced, and analyzed by TIDE analysis as described above.

Statistical Analysis: Data were analyzed with GraphPad Prism 5 and presented as arithmetic mean ± standard deviation (SD) of at least triplicates. The statistical significance of the experiments was determined using the two-tailed student's t-test, $****p \leq 0.0001$, $***p \leq 0.001$, $**p \leq 0.01$, $*p \leq 0.05$.

Supporting Information

Supporting Information is available from the Wiley Online Library or from the author.

Acknowledgements

The authors acknowledge support by the UPGRADE (Unlocking Precision Gene Therapy) project that has received funding from the European Union's Horizon 2020 research and innovation programme under grant agreement No 825825. This work was also supported by the German Research Foundation (DFG) SFB1032 (project-ID 201269156) sub-project B4. Y.L., X.L., and H.M. appreciate the fellowship of the China Scholarship Council that supports their Ph.D. studies. U.L. appreciates support from the Galenus Foundation (Vienna, Austria). The authors thank Özgür Öztürk for performing TEM measurements, and Teoman Benli-Hoppe for performing MALDI-TOF mass spectrometry measurements. TOC figure and some graphical elements in Figure 6c, Figure 7a, and Figure 8a were created with Biorender.com.

Conflict of Interest

The authors declare no conflict of interest.

Author Contributions

Y.L.: Conceptualization, Methodology, Validation, Investigation, Writing – original draft. U.W.: Methodology, Validation, Investigation. J.P.: Methodology, Validation, Investigation. E.H.: Methodology, Validation, Investigation. M.H.: Methodology, Validation, Investigation. X.L.: Methodology, Validation, Investigation. H.M.: Methodology, Validation, Investigation. E.W.: Conceptualization, Supervision, Funding acquisition, Writing – original draft. U.L.: Conceptualization, Supervision, Funding acquisition, Writing – original draft.

Data Availability Statement

The data that support the findings of this study are available from the corresponding author upon reasonable request.

Keywords

cellular delivery, clustered regularly interspaced short palindromic repeats/ clustered regularly interspaced short palindromic repeats-associated protein 9, folate receptors, gene editing, nanocarriers

Received: August 29, 2022
Revised: October 17, 2022
Published online:

[1] a) L. Cong, F. A. Ran, D. Cox, S. Lin, R. Barretto, N. Habib, D. Hsu Patrick, X. Wu, W. Jiang, A. Marraffini Luciano, F. Zhang, *Science* **2013**, *339*, 819; b) P. D. Hsu, E. S. Lander, F. Zhang, *Cell* **2014**, *157*, 1262; c) A. Doudna Jennifer, E. Charpentier, *Science* **2014**, *346*, 1258096.

[2] A. Katti, B. J. Diaz, C. M. Caragine, N. E. Sanjana, L. E. Dow, *Nat. Rev. Cancer* **2022**, *22*, 259.

[3] S. C. Wei, C. R. Duffy, J. P. Allison, *Cancer Discovery* **2018**, *8*, 1069.

[4] P. Darvin, S. M. Toor, V. Sasidharan Nair, E. Elkord, *Exp. Mol. Med.* **2018**, *50*, 1.

[5] a) F. S. Hodi, S. J. O'Day, D. F. McDermott, R. W. Weber, J. A. Sosman, J. B. Haanen, R. Gonzalez, C. Robert, D. Schadendorf, J. C. Hassel, W. Akerley, A. J. M. van den Eertwegh, J. Lutzky, P. Lorigan, J. M. Vaubel, G. P. Linette, D. Hogg, C. H. Ottensmeier, C. Lebbé, C. Peschel, I. Quirt, J. I. Clark, J. D. Wolchok, J. S. Weber, J. Tian, M. J. Yellin, G. M. Nichol, A. Hoos, W. J. Urba, *N. Engl. J. Med.* **2010**, *363*, 711; b) C. Robert, L. Thomas, I. Bondarenko, S. O'Day, J. Weber, C. Garbe, C. Lebbe, J.-F. Baurain, A. Testori, J.-J. Grob, N. Davidson, J. Richards, M. Maio, A. Hauschild, W. H. Miller, P. Gascon, M. Lotem, K. Harmankaya, R. Ibrahim, S. Francis, T.-T. Chen, R. Humphrey, A. Hoos, J. D. Wolchok, *N. Engl. J. Med.* **2011**, *364*, 2517.

[6] a) A. B. El-Khoueiry, B. Sangro, T. Yau, T. S. Crocenzi, M. Kudo, C. Hsu, T.-Y. Kim, S.-P. Choo, J. Trojan, T. H. Welling, T. Meyer, Y.-K. Kang, W. Yeo, A. Chopra, J. Anderson, C. dela Cruz, L. Lang, J. Neely, H. Tang, H. B. Dastani, I. Melero, *Lancet* **2017**, *389*, 2492; b) S. M. Ansell, A. M. Lesokhin, I. Borrello, A. Halwani, E. C. Scott, M. Gutierrez, S. J. Schuster, M. M. Millenson, D. Cattry, G. J. Freeman, S. J. Rodig, B. Chapuy, A. H. Ligon, L. Zhu, J. F. Grosso, S. Y. Kim, J. M. Timmerman, M. A. Shipp, P. Armand, *N. Engl. J. Med.* **2014**, *372*, 311.

[7] a) M. A. Socinski, R. M. Jotte, F. Cappuzzo, F. Orlandi, D. Stroyakovskiy, N. Nogami, D. Rodríguez-Abreu, D. Moro-Sibilot, C. A. Thomas, F. Barlesi, G. Finley, C. Kelsch, A. Lee, S. Coleman, Y. Deng, Y. Shen, M. Kowanetz, A. Lopez-Chavez, A. Sandler, M. Reck, *N. Engl. J. Med.* **2018**, *378*, 2288; b) P. Schmid, S. Adams, H. S. Rugo, A. Schneeweiss, C. H. Barrios, H. Iwata, V. Diéras, R. Hegg, S.-A. Im, G. S. Wright, V. Henschel, L. Molinero, S. Y. Chui, R. Funke, A. Husain, E. P. Winer, S. Loi, L. A. Emens, *N. Engl. J. Med.* **2018**, *379*, 2108.

[8] a) L. Liu, X. You, S. Han, Y. Sun, J. Zhang, Y. Zhang, *Oncol. Rep.* **2021**, *45*, 835; b) K. Mahnke, A. H. Enk, *J. Invest. Dermatol.* **2016**, *136*, 9; c) L. Gorvel, D. Olive, *F1000Res.* **2020**, *9*, 354.

[9] H. Stamm, L. Oliveira-Ferrer, E.-M. Grossjohann, J. Muschhammer, V. Thaden, F. Brauneck, R. Kischel, V. Müller, C. Bokemeyer, W. Fiedler, J. Wellbrock, *Oncoimmunology* **2019**, *8*, e1674605.

[10] C. Zhang, Y. Wang, X. Xun, S. Wang, X. Xiang, S. Hu, Q. Cheng, J. Guo, Z. Li, J. Zhu, *J. Immunother.* **2020**, *43*, 236.

[11] L. Wu, L. Mao, J.-F. Liu, L. Chen, G.-T. Yu, L.-L. Yang, H. Wu, L.-L. Bu, A. B. Kulkarni, W.-F. Zhang, Z.-J. Sun, *Cancer Immunol. Res.* **2019**, *7*, 1700.

[12] S. Li, J. Ding, Y. Wang, X. Wang, L. Lv, *J. Gastroenterol. Hepatol.* **2022**, *37*, 154.

[13] T. Inozume, T. Yaguchi, J. Furuta, K. Harada, Y. Kawakami, S. Shimada, *J. Invest. Dermatol.* **2016**, *136*, 255.
[14] P. Kučan Brlić, T. Lenac Roviš, G. Cinamon, P. Tsukerman, O. Mandelboim, S. Jonjić, *Cell Mol. Immunol.* **2019**, *16*, 40.
[15] a) K. E. Sloan, J. K. Stewart, A. F. Treloar, R. T. Matthews, D. G. Jay, *Cancer Res.* **2005**, *65*, 10930; b) K. E. Sloan, B. K. Eustace, J. K. Stewart, C. Zehetmeier, C. Torella, M. Simeone, J. E. Roy, C. Unger, D. N. Louis, L. L. Ilag, D. G. Jay, *BMC Cancer* **2004**, *4*, 73; c) T. Kono, Y. Imai, S.-i. Yasuda, K. Ohmori, H. Fukui, K. Ichikawa, S. Tomita, J. Imura, Y. Kuroda, Y. Ueda, T. Fujimori, *Int. J. Cancer* **2008**, *122*, 317.
[16] a) S. Tane, Y. Maniwa, D. Hokka, S. Tauchi, W. Nishio, Y. Okita, M. Yoshimura, *Exp. Mol. Pathol.* **2013**, *94*, 330; b) Q. Zheng, B. Wang, J. Gao, N. Xin, W. Wang, X. Song, Y. Shao, C. Zhao, *J. Cell. Mol. Med.* **2018**, *22*, 131.
[17] X. Ou, Q. Ma, W. Yin, X. Ma, Z. He, *Front. Cell Dev. Biol.* **2021**, *9*, 674467.
[18] M. Conroy, J. Naidoo, *Nat. Commun.* **2022**, *13*, 392.
[19] Y. Lin, E. Wagner, U. Lächelt, *Biomater. Sci.* **2022**, *10*, 1166.
[20] a) E. Kouranova, K. Forbes, G. Zhao, J. Warren, A. Bartels, Y. Wu, X. Cui, *Hum. Gene Ther.* **2016**, *27*, 464; b) R. Kumar, C. F. Santa Chalarca, M. R. Bockman, C. V. Bruggen, C. J. Grimme, R. J. Dalal, M. G. Hanson, J. K. Hexum, T. M. Reineke, *Chem. Rev.* **2021**, *121*, 11527.
[21] a) R. Rouet, B. A. Thuma, M. D. Roy, N. G. Lintner, D. M. Rubitski, J. E. Finley, H. M. Wisniewska, R. Mendonsa, A. Hirsh, L. de Oñate, J. Compte Barrón, T. J. McLellan, J. Bellenger, X. Feng, A. Varghese, B. A. Chrunyk, K. Borzilleri, K. D. Hesp, K. Zhou, N. Ma, M. Tu, R. Dullea, K. F. McClure, R. C. Wilson, S. Liras, V. Mascitti, J. A. Doudna, *J. Am. Chem. Soc.* **2018**, *140*, 6596; b) J. R. Hamilton, C. A. Tsuchida, D. N. Nguyen, B. R. Shy, E. R. McGarrigle, C. R. Sandoval Espinoza, D. Carr, F. Blaeschke, A. Marson, J. A. Doudna, *Cell Rep.* **2021**, *35*, 109207; c) L. Zhang, L. Wang, Y. Xie, P. Wang, S. Deng, A. Qin, J. Zhang, X. Yu, W. Zheng, X. Jiang, *Angew. Chem., Int. Ed.* **2019**, *58*, 12404.
[22] a) L. Hartmann, E. Krause, M. Antonietti, H. G. Börner, *Biomacromolecules* **2006**, *7*, 1239; b) L. Hartmann, H. G. Börner, *Adv. Mater.* **2009**, *21*, 3425.
[23] S. Berger, A. Krhač Levačić, E. Hörterer, U. Wilk, T. Benli-Hoppe, Y. Wang, Ö. Öztürk, J. Luo, E. Wagner, *Biomacromolecules* **2021**, *22*, 1282.
[24] a) J. Luo, M. Höhn, S. Reinhard, D. M. Loy, P. M. Klein, E. Wagner, *Adv. Funct. Mater.* **2019**, *29*, 1900697; b) J. Luo, J. Schmaus, M. Cui, E. Hörterer, U. Wilk, M. Höhn, M. Däther, S. Berger, T. Benli-Hoppe, L. Peng, E. Wagner, *J. Controlled Release* **2021**, *329*, 919.
[25] A. Krhač Levačić, S. Berger, J. Müller, A. Wegner, U. Lächelt, C. Dohmen, C. Rudolph, E. Wagner, *J. Controlled Release* **2021**, *339*, 27.
[26] a) P. Zhang, D. He, P. M. Klein, X. Liu, R. Röder, M. Döblinger, E. Wagner, *Adv. Funct. Mater.* **2015**, *25*, 6627; b) P. Zhang, B. Steinborn, U. Lächelt, S. Zahler, E. Wagner, *Biomacromolecules* **2017**, *18*, 2509.
[27] J. Kuhn, P. M. Klein, N. Al Danaf, J. Z. Nordin, S. Reinhard, D. M. Loy, M. Höhn, S. El Andaloussi, D. C. Lamb, E. Wagner, Y. Aoki, T. Lehto, U. Lächelt, *Adv. Funct. Mater.* **2019**, *29*, 1906432.
[28] J. Kuhn, Y. Lin, A. Krhac Levacic, N. Al Danaf, L. Peng, M. Höhn, D. C. Lamb, E. Wagner, U. Lächelt, *Bioconjugate Chem.* **2020**, *31*, 729.
[29] a) T. Benli-Hoppe, Ş. Göl Öztürk, Ö. Öztürk, S. Berger, E. Wagner, M. Yazdi, *Macromol. Rapid Commun.* **2022**, *43*, 2100602; b) P. M. Klein, S. Kern, D.-J. Lee, J. Schmaus, M. Höhn, J. Gorges, U. Kazmaier, E. Wagner, *Biomaterials* **2018**, *178*, 630; c) Y. Wang, J. Luo, I. Truebenbach, S. Reinhard, P. M. Klein, M. Höhn, S. Kern, S. Morys, D. M. Loy, E. Wagner, W. Zhang, *ACS Biomater. Sci. Eng.* **2020**, *6*, 1074.
[30] S. Reinhard, W. Zhang, E. Wagner, *ChemMedChem* **2017**, *12*, 1464.
[31] a) X. Guan, Z. Guo, T. Wang, L. Lin, J. Chen, H. Tian, X. Chen, *Biomacromolecules* **2017**, *18*, 1342; b) T. Takahashi, Y. Yamada, K. Kataoka, Y. Nagasaki, *J. Controlled Release* **2005**, *107*, 408; c) C. Zhu, M. Zheng, F. Meng, F. M. Mickler, N. Ruthardt, X. Zhu, Z. Zhong, *Biomacromolecules* **2012**, *13*, 769; d) Y. Nie, M. Günther, Z. Gu, E. Wagner, *Biomaterials* **2011**, *32*, 858.
[32] T. G. F. Souza, V. S. T. Ciminelli, N. D. S. Mohallem, *J. Phys.: Conf. Ser.* **2016**, *733*, 012039.
[33] a) W. Zhang, Q. Cheng, S. Guo, D. Lin, P. Huang, J. Liu, T. Wei, L. Deng, Z. Liang, X.-J. Liang, A. Dong, *Biomaterials* **2013**, *34*, 6495; b) M. Noga, D. Edinger, R. Kläger, S. V. Wegner, J. P. Spatz, E. Wagner, G. Winter, A. Besheer, *Biomaterials* **2013**, *34*, 2530.
[34] R. G. W. Anderson, B. A. Kamen, K. G. Rothberg, S. W. Lacey, *Science* **1992**, *255*, 410.
[35] a) J. J. Turek, C. P. Leamon, P. S. Low, *J. Cell Sci.* **1993**, *106*, 423; b) R. J. Lee, S. Wang, P. S. Low, *Biochim. Biophys. Acta, Mol. Cell Res.* **1996**, *1312*, 237.
[36] Y. Rui, R. Wilson David, Y. Tzeng Stephany, M. Yamagata Hannah, D. Sudhakar, M. Conge, A. Berlinicke Cynthia, J. Zack Donald, A. Tuesca, J. Green Jordan, *Sci. Adv.* **2022**, *8*, eabk2855.
[37] A. Wittrup, A. Ai, X. Liu, P. Hamar, R. Trifonova, K. Charisse, M. Manoharan, T. Kirchhausen, J. Lieberman, *Nat. Biotechnol.* **2015**, *33*, 870.
[38] D. Masson, A. Jarry, B. Baury, P. Blanchardie, C. Laboisse, P. Lustenberger, M. G. Denis, *Gut* **2001**, *49*, 236.
[39] M. Efremova, D. Rieder, V. Klepsch, P. Charoentong, F. Finotello, H. Hackl, N. Hermann-Kleiter, M. Löwer, G. Baier, A. Krogsdam, Z. Trajanoski, *Nat. Commun.* **2018**, *9*, 32.
[40] D. Schaffert, N. Badgujar, E. Wagner, *Org. Lett.* **2011**, *13*, 1586.
[41] S. Ramakrishna, A.-B. Kwaku Dad, J. Beloor, R. Gopalappa, S.-K. Lee, H. Kim, *Genome Res.* **2014**, *24*, 1020.